Technical Report No. 32-28

Analysis of Radio-Command Mid-Course Guidance

A. R. M. Noton
E. Cutting
F. L. Barnes

JET PROPULSION LABORATORY
CALIFORNIA INSTITUTE OF TECHNOLOGY
PASADENA, CALIFORNIA

September 8, 1960

1 of 30

NATIONAL AERONAUTICS AND SPACE ADMINISTRATION
CONTRACT NO. NASw-6

Technical Report No. 32-28

Analysis of Radio-Command Mid-Course Guidance

A. R. M. Noton
E. Cutting
F. L. Barnes

C. R. Gates

C. R. Gates, Chief
Systems Analysis

JET PROPULSION LABORATORY
CALIFORNIA INSTITUTE OF TECHNOLOGY
PASADENA, CALIFORNIA

September 8, 1960

2

CONTENTS

I. Introduction 1

II. Theory of Mid-Course Maneuvers 1
- A. Guidance Equations 1
- B. Calculation of Differential Coefficients 4
- C. In-Flight Calculations of the Mid-Course Maneuver 4
- D. Statistical Calculation of the Required Maneuver 5
- E. Error Analyses of Mid-Course Guidance Systems 6

III. Orbit Determination From Radio Measurements 7
- A. Summary 7
- B. Tracking System 7
- C. Orbit-Determination Program 8
- D. Accuracy of Tracking Data 9
- E. Results 11
- F. Further Results 12

IV. Guidance Systems 15

V. Conclusions 18

Appendixes
- A. Correcting Velocity Components 18
- B. Minimization of the Magnitude of the Maneuver 19
- C. Probability-Density Function of the Magnitude of the Mid-Course Maneuver 19
- D. Computation of the Orbit From Radio Tracking Data 20

References 23

Blank page

TABLES

1. Mid-course maneuver for 99% of all cases 6
2. Assumed noise characteristics 10
3. Possible mid-course guidance systems 15
4. Representative figures for the accuracy of mid-course guidance (rms quotations of errors) 18

FIGURES

1. Definition of miss components M_1 and M_2 2
2. Definition of miss components $B \cdot R$ and $B \cdot T$ 2
3. Vectors relevant to the analysis of single-impulse mid-course maneuvers 3
4. Miss at the Moon due to radio tracking errors 11
5. Miss at Venus and Mars due to radio tracking errors 11
6. Accuracy of orbit determination with mid-course maneuver 12
7. Accuracy of orbit determination with range data 12
8. Effect of range-rate accuracy on major miss component 13
9. Effect of angle accuracy on major miss component 13
10. Miss at the Moon due to radio tracking errors as a function of total number of measurements 14
11. Mid-course maneuver to correct injection errors 16
12. Mid-course maneuver for the *Agena–Discoverer* guidance system . . . 17
13. Variation of flight time and impact speed when only miss components are corrected by a maneuver in the critical plane (trajectory and guidance as in Fig. 12) 17
14. Coefficients relating miss at the Moon to errors in magnitude and direction of mid-course maneuver 17
15. Coefficients relating speed at the Moon to errors in magnitude and direction of mid-course maneuver 17
C-1. Probability-density functions of the magnitude of a mid-course maneuver when restricted to a plane 20

ABSTRACT

The injection or ascent guidance systems that will be used for space vehicles in the next few years will not have sufficient accuracy for advanced lunar or interplanetary missions. It will be necessary to have some form of mid-course guidance in order to reduce terminal dispersions.

This Report is concerned with a specific mid-course guidance scheme which utilizes a small rocket motor mounted on the spacecraft for small impulse-type corrections. Magnitude and directions of the correcting impulse is computed on the ground from radio tracking measurements, and appropriate commands are transmitted to the probe. The Report first developed the mathematical theory of mid-course guidance. Terminal coordinates are discussed, the concept of the critical plane is introduced, and the exact computation of the maneuver is covered in addition to the method of estimating the required amount of rocket propellant. A thorough error analysis of the mid-course guidance system is presented. The effects of pointing and shut-off errors of the rocket motor are determined. A detailed study is made of the errors associated with the computation of the mid-course correction from the noisy tracking data. The theory is applied in representative cases, and many numerical results are shown.

7

I. INTRODUCTION

The injection or ascent guidance systems that will be used for space vehicles in the next few years will not have sufficient accuracy for advanced lunar or interplanetary missions. Some form of post-injection guidance will be necessary to reduce the dispersion at the destination; such guidance may be accomplished by means of self-contained systems or with Earth-based measurements.

The accuracy of self-contained systems tends to improve in the vicinity of the destination, and such systems are not susceptible to hostile "jamming." However, the equipment in the spacecraft is much simpler in the case of Earth-based guidance systems, and jamming is not considered a menace to NASA space vehicles. Furthermore, long-term studies at the Jet Propulsion Laboratory (JPL) have revealed that a system of mid-course guidance based on radio measurements and command can provide surprising accuracy for both lunar and planetary missions. Such radio-command guidance also takes advantage of the complex of deep-space tracking sites that are being set up in California, Australia, and Africa. Such guidance (with relatively simple payload equipment) has, therefore, been chosen for later spacecraft in the *Ranger* program both for the Moon and for the planets.

This Report first develops the theoretical structure of mid-course guidance. Terminal coordinates are discussed, the concept of the critical plane is introduced, and the exact computation of the maneuver is covered in addition to the method of estimating the required amount of rocket propellant. In considering the errors of a mid-course guidance system, a detailed study has been made of the errors associated with the computation of the orbit (prior to the maneuver). Radar tracking data are contaminated with noise, which naturally degrades the precision of the orbit determination. The method of determining the orbit is outlined, followed by the error analyses that have been applied.

Finally, systems of mechanization are discussed and a number of representative results presented (e.g., the required maneuver for a given injection-guidance system and the accuracy that can be anticipated at the Moon, Mars, and Venus).

II. THEORY OF MID-COURSE MANEUVERS

A. Guidance Equations

At this point, it is convenient to assume that the actual trajectory followed by a vehicle differs only slightly from some precalculated standard trajectory. Linear perturbation theory may then be applied to all calculations dealing with coordinate variations and small velocity increments (for correcting the trajectory). Although for most purposes the approximations of linear perturbations are good, the theory is invoked more as a convenience than as a necessary step in the calculations. The theory is used to carry out first-order analyses but, where necessary, iterative procedures should be used to refine the approximations.

If a probe reaches the desired destination point at a given time t_2 on the ideal or standard trajectory, then, because of injection errors, the probe will generally not reach the same point at time t_2 on an actual trajectory unless some correction is applied. Let the difference in the coordinates of position on the standard and the actual trajectory (in the absence of a correction) be δx, δy, and δz at time t_2. It is shown in Appendix A that, in order to correct the trajectory by applying a velocity impulse with components V_x, V_y, and V_z at some previous time t_1,

$$\begin{bmatrix} \delta x \\ \delta y \\ \delta z \end{bmatrix}_{t_2} = -H \begin{bmatrix} V_x \\ V_y \\ V_z \end{bmatrix}_{t_1} \tag{1}$$

where H is a 3×3 matrix, the elements of which can be determined from computations on the standard trajectory for any given t_1 and t_2. Components δx, δy, and δz at time t_2 can be computed indirectly from measured data; thus, the three velocity components necessary for the correction of the trajectory are determined by Eq. 1. This

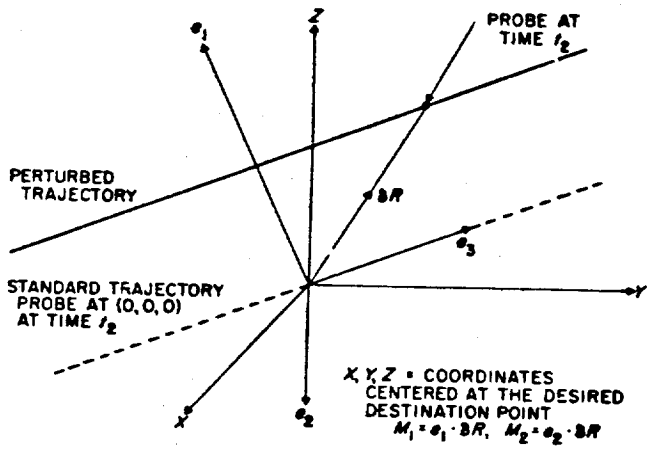

Figure 1. Definition of miss components M_1 and M_2

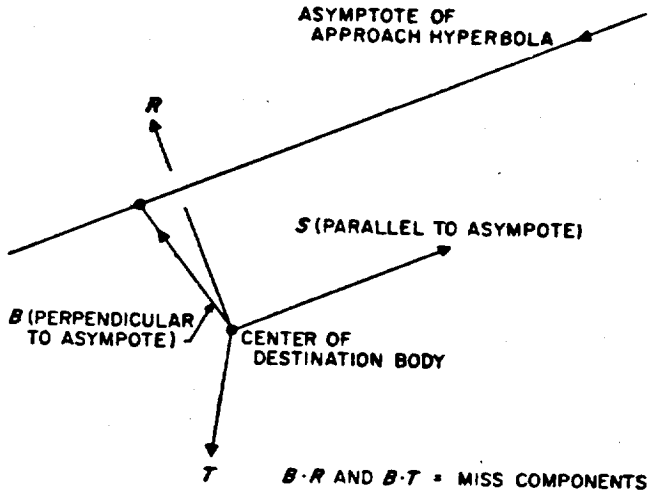

Figure 2. Definition of miss components $B \cdot R$ and $B \cdot T$.

would, however, guide the space probe to intercept a given (moving) point in space at the given time t_2. The latter restriction would often be unnecessary, since small variations in the flight time may be permissible.

In order to allow variations of flight time, a new set of rectangular axes is taken (Fig. 1), centered at the probe position at time t_2 on the standard trajectory. The new axes are defined by the unit base vectors e_1, e_2, and e_3, where e_3 lies along the probe velocity vector at time t_2 on the standard trajectory. Since e_2 is in the xy-plane and perpendicular to e_3 and e_1, it completes the set of mutually perpendicular base vectors. If, then, δR is the vector displacement corresponding to δx, δy, and δz at time t_2, three new miss components may be defined:

$$M_1 = e_1 \cdot \delta R, \quad M_2 = e_2 \cdot \delta R, \quad M_3 = e_3 \cdot \delta R \qquad (2)$$

Assuming that, as a first-order approximation, perturbed trajectories have the same velocity direction at time t_2, then M_1 and M_2 are the miss components at some time different from t_2, and M_3 is associated only with time-of-flight variations. Thus,

$$\begin{bmatrix} M_1 \\ M_2 \end{bmatrix} = \begin{bmatrix} l_1 & m_1 & n_1 \\ l_2 & m_2 & n_2 \end{bmatrix} \begin{bmatrix} \delta x \\ \delta y \\ \delta z \end{bmatrix}_{t_2} \qquad (3)$$

where (l_1, m_1, n_1) and (l_2, m_2, n_2) are the direction cosines of e_1 and e_2, respectively. Indicating the 2×3 matrix of Eq. 3 by N, Eq. 1 can be modified to

$$\begin{bmatrix} M_1 \\ M_2 \end{bmatrix} = -NH \begin{bmatrix} V_x \\ V_y \\ V_z \end{bmatrix}_{t_1} \qquad (4)$$

where M_1 and M_2 are the miss components perpendicular to the terminal velocity vector (on the standard trajectory). Other terminal coordinates may, however, be appropriate to certain missions. For example, if the object of the mission is to impact the Moon at a given spot with a given speed, then it would be logical to choose actual surface miss components and speed at lunar impact. Such coordinates are not, however, defined for trajectories which miss the Moon; this difficulty may be overcome by defining impact as the intersection with the plane which is tangential to the Moon at the standard impact point. Such coordinates approach the true impact coordinates for small perturbations.

The terminal coordinates discussed above are linear functions of small perturbations applied at some earlier point in the trajectory. However, as a result of the attraction of the destination body (e.g., the Moon), departures from linearity occur with large perturbations. For this reason, another set of terminal coordinates has been introduced (Ref. 1) and used extensively at JPL, since they are linear for wide ranges of perturbation variables. They are defined in Fig. 2. Three mutually perpendicular base vectors (R, S, and T), are chosen such that S is parallel to the asymptote of the approach hyperbola. Vector T is chosen, for convenience, in the xy-plane of the trajectory computation, and R then completes the right-handed orthogonal system of axes. Vector B is the perpendicular from the center of the attracting body to the asymptote, and the two miss components are defined as $M_1 = B \cdot R$ and $M_2 = B \cdot T$. Returning to Eq. 4, M_1 and M_2 will henceforth denote miss components in general, but the reader must recognize the fact that the choice of such coordinates will depend on the particular mission and calculation. Equation 4 is, in fact, two equations, which must be satisfied by the three velocity components (V_x, V_y, and V_z) in order that the trajectory be corrected

to pass through the desired end point at some unspecified time.

The three components have to satisfy only two equations. There is one degree of redundancy, which may be used for one of the following:

(1) To minimize the magnitude of the correction

(2) To apply a geometrical constraint to the maneuver for the sake of practical convenience

(3) To control an additional destination variable such as speed or time of arrival

In the first case, let

$$NH = K = [k_{ij}] \tag{5}$$

It is shown in Appendix B that the magnitude of V_x, V_y, and V_z is a minimum when

$$K_{31}V_x + K_{32}V_y + K_{33}V_z = 0 \tag{6}$$

where K_{ij} is the cofactor of the element k_{ij}.

Equation 6 defines a plane which always contains the correcting velocity vector when applied at a given time t_1. The plane is independent of injection errors. It may be referred to as the most efficient or critical plane, the normal to that plane being the non-critical direction. The latter depends on the trajectory and the maneuver time along the trajectory.

A typical situation is illustrated in Fig. 3, where the loci of the velocity vector (relative to the Earth) and the non-critical direction are plotted on a celestial sphere for different times after injection into a 66-hr lunar orbit.

In practice, it may not be convenient to apply the correction in the critical plane. Referring to option (2) above, the correction might be restricted to a plane perpendicular to the probe–Sun axis. With a rocket mounted at right angles to that axis, one face of the spacecraft (carrying solar panels) need not then be turned away from the Sun during the mid-course maneuver.

When the rocket thrust vector is restricted to a plane, critical or otherwise, the velocity components would satisfy an equation of the form

$$aV_x + bV_y + cV_z = 0 \tag{7}$$

in addition to Eq. 4. To calculate the velocity components, a 3×3 matrix is formed from the 2×3 matrix NH and a, b, and c of Eq. 7:

$$P = \begin{bmatrix} NH \\ \hline a\ b\ c \end{bmatrix} \tag{8}$$

P being a 3×3 matrix. Then,

$$\begin{bmatrix} M_1 \\ M_2 \\ 0 \end{bmatrix} = -P \begin{bmatrix} V_x \\ V_y \\ V_z \end{bmatrix} \tag{9}$$

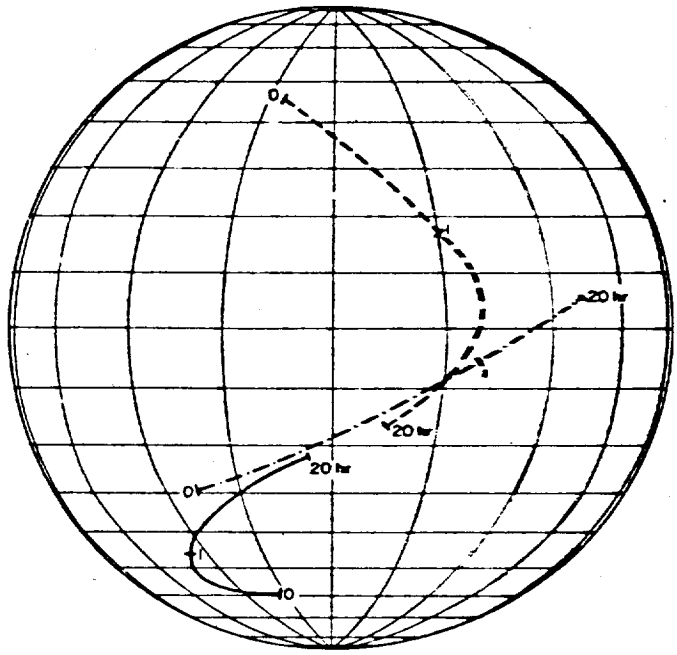

Figure 3. Vectors relevant to the analysis of single-impulse mid-course maneuvers

and

$$\begin{bmatrix} V_x \\ V_y \\ V_z \end{bmatrix} = -P^{-1} \begin{bmatrix} M_1 \\ M_2 \\ 0 \end{bmatrix} \tag{10}$$

which represents three equations specifying the velocity components (subject to a constraint) in terms of miss components M_1 and M_2. The latter would be obtained from the computed orbit according to the measured data.

Taking advantage of the degree of freedom revealed in Eq. 4, the third option would be to control some additional terminal variable, e.g., flight time or speed of arrival. Thus a 3×3 matrix K' of differential coefficients can be found, such that

$$\begin{bmatrix} M_1 \\ M_2 \\ S \end{bmatrix} = -K' \begin{bmatrix} V_x \\ V_y \\ V_z \end{bmatrix} \tag{11}$$

where S indicates the variation in the speed of arrival. (The calculations are also the same for variations in flight time.) The three velocity components are then uniquely defined by

$$\begin{bmatrix} V_x \\ V_y \\ V_z \end{bmatrix} = -(K')^{-1} \begin{bmatrix} M_1 \\ M_2 \\ S \end{bmatrix} \tag{12}$$

and for random errors in the three terminal variables, the variable-impulse mid-course rocket may have to be fixed in any direction.

It will be observed that the third row of Eq. 11 would read:

$$S \text{ or } \Delta T = -k'_{31} V_x - k'_{32} V_y - k'_{33} V_z \qquad (13)$$

depending on whether speed or flight time was being corrected. It follows that if a maneuver were made in the plane defined by

$$k'_{31} V_x + k'_{32} V_y + k'_{33} V_z = 0 \qquad (14)$$

then the third terminal coordinate (e.g., speed or flight time) would be unaffected. It also follows that the direction defined by the components (k'_{31}, k'_{32}, and k'_{33}) is the most efficient direction for correcting the third terminal coordinate, hence the term "time-critical direction" (plotted in Fig. 3). As the time-critical direction approaches the critical plane of miss components, it becomes impossible to correct for miss and flight time, since the K' matrix of Eq. 12 approaches singularity. This situation may be observed near injection in Fig. 3.

B. Calculation of Differential Coefficients

The matrices NH and K' referred to above are composed of differential coefficients which relate velocity perturbations at the maneuver point to resulting perturbations in the terminal coordinates; other coefficients must also be introduced. Although the choice of terminal coordinates has been discussed, no mention has so far been made of the method of calculating such coefficients. Several possible methods exist:

(1) Direct computation of perturbed trajectories
(2) Solution of the differential equations satisfied by the differential coefficients
(3) Solution of the adjoint equations
(4) Analytical calculation from conic formulas

Method (1) has been used extensively at JPL. In order to compute n coefficients, one standard and n perturbed trajectories must be computed (invariably on an automatic computer). Differential coefficients such as $(\partial M_1)/(\partial V_x)$ are then approximated by $(\Delta M_1)/(\Delta V_x)$. The procedure is simple to apply and, with additional perturbed trajectories, permits a check on the validity of first-order approximations. The choice of the size of the increments is important since, if the increments are too large, nonlinear effects appear, and if the increments are too small, then errors in the trajectory computation become serious.

In setting up the equations for machine-computation of trajectories, it is easy to include the differential equations which the differential coefficients themselves must satisfy. The coefficients can then be printed out during the computation of the trajectory itself (Ref. 2). Once such equations are programmed, this method (now being employed at JPL) is evidently very fast, although no check on linearity is possible.

A similar method is solution of the adjoint equations (Ref. 3). The differential equations of perturbed trajectories are set up as six simultaneous first-order linear equations. By transposing the matrix of this set of equations, another set of six equations (the adjoint set) is derived. Numerical integration of the new set then gives the differential coefficients along the trajectory. Although the functions which form the coefficients of the adjoint equations are available from the ordinary trajectory computation, the method is inconvenient, since the integration of the adjoint equations has to be in reverse time; i.e., integration starts from the end of the trajectory. Method (3) has been used only experimentally at JPL.

With reference to Method (4), trajectories can be approximated by parts of more than one conic. For example, a lunar trajectory can be approximated for most of the flight by an ellipse or hyperbola relative to the Earth; within 40,000 mi of the Moon, the trajectory approaches a hyperbola relative to the Moon. Since perturbation coefficients can be deduced analytically for such orbits, the required differential coefficients may be obtained by appropriate combinations of the coefficients calculated on the separate conics. So far, this technique has been utilized merely to provide approximate coefficients, but refined methods of calculation are being developed.

C. In-Flight Calculations of the Mid-Course Maneuver

The calculation of the mid-course maneuver to a first order of approximation is given in Eq. 10 or 12. However, if nothing more than such equations were used to compute the required maneuver, then the over-all accuracy of the guidance system would be degraded unnecessarily. It is proposed to refine the computation of the following iterative procedure:

$$\begin{bmatrix} V_x \\ V_y \\ V_z \end{bmatrix}_{n+1} = \begin{bmatrix} V_x \\ V_y \\ V_z \end{bmatrix}_n + (K')^{-1} \begin{bmatrix} M_1 \\ M_2 \\ S \end{bmatrix} \qquad (15)$$

with a similar expression in the case in which only miss components are to be corrected.

For the first iteration, M_1, M_2, and S would be obtained from the best estimate of the actual trajectory from tracking data (Part III). The first estimate of the maneuver would be

$$\begin{bmatrix} V_x \\ V_y \\ V_z \end{bmatrix}_1 = \begin{bmatrix} 0 \\ 0 \\ 0 \end{bmatrix}_0 + (K')^{-1} \begin{bmatrix} M_1 \\ M_2 \\ S \end{bmatrix}_0 \tag{16}$$

The trajectory would then be rerun from the maneuver point with the modified velocity components, the residual values of M_1, M_2, and S from the trajectory being substituted into

$$\begin{bmatrix} V_x \\ V_y \\ V_z \end{bmatrix}_2 = \begin{bmatrix} V_x \\ V_y \\ V_z \end{bmatrix}_1 + (K')^{-1} \begin{bmatrix} M_1 \\ M_2 \\ S \end{bmatrix}_1 \tag{17}$$

the second estimate of the maneuver. This procedure would continue until the residual terminal coordinates were acceptably small (e.g., 2-mi miss at the Moon).

Although strictly speaking, the elements of the K' matrix should be recomputed for each iteration, preliminary studies have indicated that it will often be sufficiently accurate to apply the K' matrix of the standard trajectory.

D. Statistical Calculation of the Required Maneuver

Since the magnitude of the mid-course maneuver depends on the injection errors and the latter are described statistically, a statistical calculation is necessary in order to estimate the required amount of rocket propellant for the mid-course rocket. The calculation is given below for the case in which only the miss components are corrected, although it is carried out in the same manner if an additional terminal coordinate is controlled.

From Eq. 4 and 5,

$$\begin{bmatrix} M_1 \\ M_2 \end{bmatrix} = -K \begin{bmatrix} V_x \\ V_y \\ V_z \end{bmatrix} \tag{18}$$

If the maneuver is restricted to a plane and the two perpendicular velocity components in that plane are u_1 and u_2, then an orthogonal matrix G can be found, such that

$$\begin{bmatrix} V_x \\ V_y \\ V_z \end{bmatrix} = G \begin{bmatrix} u_1 \\ u_2 \\ u_3 \end{bmatrix} \tag{19}$$

u_3 being the component normal to the plane and postulated to be zero.

Hence,

$$\begin{bmatrix} M_1 \\ M_2 \end{bmatrix} = -KG \begin{bmatrix} u_1 \\ u_2 \\ 0 \end{bmatrix} \tag{20}$$

or

$$\begin{bmatrix} M_1 \\ M_2 \end{bmatrix} = -Q \begin{bmatrix} u_1 \\ u_2 \end{bmatrix} \tag{21}$$

where Q is obtained from KG by simply omitting the third column.

Now, let δX be a 6×1 matrix of the six injection errors; then, the resulting miss components are given by

$$\begin{bmatrix} M_1 \\ M_2 \end{bmatrix} = W \delta X \tag{22}$$

where the 2×6 matrix W is composed of differential coefficients relating injection to terminal coordinates. If u_1 and u_2 are to correct such injection deviations,

$$\begin{bmatrix} u_1 \\ u_2 \end{bmatrix} = Q^{-1} W \delta X \tag{23}$$

and by multiplying each side of Eq. 23 by its transpose,

$$\begin{bmatrix} u_1^2 & u_1 u_2 \\ u_2 u_1 & u_2^2 \end{bmatrix} = Q^{-1} W \delta X \delta X^T W^T Q^{-1T} \tag{24}$$

Let the six injection errors δX now be considered as random variables; the ensemble average of Eq. 24 is

$$\begin{bmatrix} \overline{u_1^2} & \overline{u_1 u_2} \\ \overline{u_2 u_1} & \overline{u_2^2} \end{bmatrix} = Q^{-1} W \overline{(\delta X \delta X^T)} W^T Q^{-1T} \tag{25}$$

But $\overline{\delta X \, \delta X^T} = \Lambda$ is, in fact, the moment matrix of injection errors; it gives the variances and covariances of those errors and would be calculated (Ref. 4) from the form of the injection guidance system. Therefore,

$$\begin{bmatrix} \overline{u_1^2} & \overline{u_1 u_2} \\ \overline{u_2 u_1} & \overline{u_2^2} \end{bmatrix} = Q^{-1} W \Lambda W^T Q^{-1T} \tag{26}$$

and the mean-squared value of the mid-course maneuver is

$$\overline{u^2} = \overline{u_1^2 + u_2^2} = \overline{u_1^2} + \overline{u_2^2} \tag{27}$$

i.e., the sum of the two diagonal terms of the matrix on the right side of equation (26).

Now, although u_1 and u_2 satisfy a joint gaussian distribution [assuming that the injection errors satisfy a six-dimensional gaussian distribution (Ref. 4)], the distribution of $\sqrt{u_1^2 + u_2^2}$ is not gaussian. The calculation of the probability-density function of the magnitude of the maneuver is given in Appendix C (and the functions are plotted in Fig. C-1). It is shown that, in order to cope with

99 per cent of all cases, the maneuver must be N times the rms value (from Eq. 27), where N is a function of the ratio of the major to minor axes of the dispersion ellipse of velocity components in the (u_1, u_2) plane. The calculations are given in Appendix C and some values for N are given in Table 1.

Table 1. Mid-course maneuver for 99% of all cases

Ratio of major to minor axis of u_1u_2 dispersion ellipse	N, ratio of required maneuver to rms maneuver
1	2.14
3	2.52
10	2.58

E. Error Analyses of Mid-Course Guidance Systems

The sources of error in a mid-course guidance system are as follows:

(1) The orbit is not determined perfectly from radio tracking.

(2) Angular errors are introduced in pointing the mid-course rocket.

(3) The magnitude of the maneuver is in error.

The precision of orbit determination based upon radio tracking is discussed fully in Part III; only the second and third sources of error are therefore considered here. In the case in which a mid-course maneuver corrects terminal miss components and speed, Eq. 11 applies. It is, however, convenient to use a rotation matrix G to transform the components (V_x, V_y, and V_z) to the orthogonal set (u_1, u_2, and u_3), where u_3 lies along the non-critical direction. Thus,

$$\begin{bmatrix} M_1 \\ M_2 \\ S \end{bmatrix} = -(K'G) \begin{bmatrix} u_1 \\ u_2 \\ u_3 \end{bmatrix} \tag{28}$$

The coordinates V, ζ, and η are introduced, defined by

$$\begin{aligned} u_1 &= V \cos\zeta \cos\eta \\ u_2 &= V \cos\zeta \sin\eta \\ u_3 &= V \sin\zeta \end{aligned} \tag{29}$$

The errors δM_1, δM_2, and δS due to errors δV, $\delta\zeta$, and $\delta\eta$ are given by

$$\begin{bmatrix} \delta M_1 \\ \delta M_2 \\ \delta S \end{bmatrix} = -(K'G) \begin{bmatrix} V(-\sin\zeta\cos\eta\delta\zeta - \cos\zeta\sin\eta\delta\eta) + \delta V\cos\zeta\cos\eta \\ V(-\sin\zeta\sin\eta\delta\zeta + \cos\zeta\cos\eta\delta\eta) + \delta V\cos\zeta\sin\eta \\ V\cos\zeta\delta\zeta + \delta V\sin\zeta \end{bmatrix} \tag{30}$$

Let

$$(K'G) = \begin{bmatrix} a_{11} & a_{12} & 0 \\ a_{21} & a_{22} & 0 \\ a_{31} & a_{32} & a_{33} \end{bmatrix} \tag{31}$$

(a_{13} and a_{23} are zero, since u_3 is the non-critical direction.) Then, the equation for δM_1 is

$$\begin{aligned} \delta M_1 = &-(-a_{11}\sin\zeta\cos\eta - a_{12}\sin\zeta\sin\eta)V\delta\zeta \\ &-(-a_{11}\cos\zeta\sin\eta + a_{12}\cos\zeta\cos\eta)V\delta\eta \\ &-(a_{11}\cos\zeta\cos\eta + a_{12}\cos\zeta\sin\eta)\delta V \end{aligned} \tag{32}$$

The quantity $\overline{\delta M_1^2}$ is required where the errors δV, $\delta\zeta$, and $\delta\eta$ are random variables.

The rigorous analysis is beyond the scope of this Report; instead, in order to arrive at a tractable solution, some crude averaging procedures are applied; viz., V is treated as a constant equal to the average magnitude of the maneuver, and δV, $\delta\zeta$, and $\delta\eta$ are treated as uncorrelated errors. The approximation of a maneuver equally likely in any direction is also introduced. With such approximations, and after some manipulation of Eq. 32 and the corresponding equations for δM_2 and δS,

$$\overline{\delta M_1^2} + \overline{\delta M_2^2} = \lambda^2(\overline{\delta V^2} + V^2\overline{\delta\zeta^2} + V^2\overline{\delta\eta^2}) \tag{33}$$

where

$$\lambda = \sqrt{\frac{a_{11}^2 + a_{12}^2 + a_{21}^2 + a_{22}^2}{4}} \tag{34}$$

$$\overline{\delta S^2} = \mu_V^2\overline{\delta V^2} + \mu_\zeta^2 V^2\overline{\delta\zeta^2} + \mu_\eta^2 V^2\overline{\delta\eta^2} \tag{35}$$

where

$$\mu_V = \sqrt{\frac{a_{21}^2 + a_{22}^2 + 2a_{33}^2}{4}} = \mu_\zeta \tag{36}$$

$$\mu_\eta = \sqrt{\frac{a_{21}^2 + a_{22}^2}{4}} \tag{37}$$

The analysis is carried out similarly, when only the miss components are corrected.

In addition to errors in applying the maneuver, one other kind of terminal dispersion is of interest. If only the miss components are corrected, flight-time or speed variations occur, not only due to injection errors but as a result of the mid-course maneuver itself. The calculation of such variations is given below, the analysis being exactly the same in case of speed variations.

Let u_1 and u_2 be the velocity components in the plane used for correcting only miss components (Eq. 21) and δX the 6×1 matrix of injection errors (Eq. 22).

Thus,

$$Q\begin{bmatrix} u_1 \\ u_2 \end{bmatrix} = W\delta X \tag{38}$$

Let $\Delta T'$ be the flight-time variation due to injection errors; then,

$$\begin{bmatrix} M_1 \\ M_2 \\ \Delta T' \end{bmatrix} = + \begin{bmatrix} W \\ \overline{W_1} \end{bmatrix} \delta X \tag{39}$$

where W_1 is a 1×6 matrix. Let $\Delta T''$ be the flight-time variation due to the maneuver itself:

$$\Delta T'' = -Q_1 \begin{bmatrix} u_1 \\ u_2 \end{bmatrix} \tag{40}$$

where Q_1 is a 1×2 matrix. Then the total flight-time change is

$$\Delta T = \Delta T' + \Delta T'' = W_1 \delta X - Q_1 \begin{bmatrix} u_1 \\ u_2 \end{bmatrix} \tag{41}$$

But

$$\begin{bmatrix} u_1 \\ u_2 \end{bmatrix} = Q^{-1} \begin{bmatrix} M_1 \\ M_2 \end{bmatrix} = Q^{-1} W \delta X \tag{42}$$

Therefore,

$$\Delta T = (W_1 - Q_1 Q^{-1} W)\,\delta X$$

and

$$\Delta T^2 = (W_1 - Q_1 Q^{-1} W)\,\Lambda\,(W_1 - Q_1 Q^{-1} W)^T \tag{43}$$

where Λ is the moment matrix of injection errors (Eq. 25).

III. ORBIT DETERMINATION FROM RADIO MEASUREMENTS

A. Summary

In the radio-command mid-course guidance system, radio tracking stations at several locations on the Earth track the spacecraft along its orbit, measuring quantities such as doppler shift and tracking angles. Measurements from different stations are transmitted to a central computing facility which determines the orbit that fits the measured data with the least-square error. This coasting orbit can be completely specified by six coordinates at a given time (for example, three components of position and three components of velocity at nominal injection time). From the measured orbit, the central computer determines the mid-course impulse required to correct quantities such as miss components and time of flight at the target. Appropriate attitude and velocity increment commands are then transmitted to the spacecraft from one of the tracking sites. Tracking continues after the maneuver, since the orbit must be redetermined for evaluation purposes, scientific experiments, and possibly a retro-maneuver.

It can be seen that the radio tracking system and central computer effectively close the loop in this guidance system. As in all closed-loop systems, the measurements of the controlled quantities are contaminated by noise. For example, angle-tracking data are subject to random errors due to receiver noise, which causes jitter in the antenna servos. Although only a few radio measurements are sufficient to determine an orbit, the accuracy of the orbit determination is greatly improved by appropriately smoothing a large number of data points from different sites. For error analysis of the mid-course guidance system, it is necessary to find out how accurately the orbit is determined from measured data. In this Part, the tracking system and orbit-determination program are described. The method of finding the accuracy of orbit determination is developed, and representative results are shown in the graphs. Also, the effect of changing various parameters of the tracking system on the accuracy of orbit determination is studied.

B. Tracking System

Most of the data for lunar and interplanetary orbit determination will be obtained from the NASA Deep Space Net (Ref. 5). As presently planned, the tracking net will consist of three tracking stations, spaced on the Earth in such a way that a spacecraft which is at least several Earth radii from the Earth will always be visible from at least one station. It is planned that each station will eventually include a high-gain directive receiving antenna with accurate positioning servos, a sensitive low-noise receiver, a transmitter, and a suitable antenna. Also, there will be data processing equipment and facilities for real-time communication of data to the NASA computing and control center. The first Deep Space Net (DSN) station at Goldstone Lake in California is operational at the present time. It is planned that the other two stations will be located in South Africa and Australia and will be operational in 1963 and 1964, respectively.

The Goldstone tracking station, which was used in tracking *Pioneer IV*, is a prototype of the other DSN stations. The tracking equipment at Goldstone is described in detail in Ref. 6. The receiving antenna is a polar-mounted, 85-ft-diameter, parabolic reflector, which was originally designed for radio-astronomy research. The antenna is equipped with an accurate servo-drive system and uses simultaneous lobing for automatic tracking. The receiver is a low-noise, 960-mc, narrow-band, phase-tracking, double-conversion superheterodyne with a data channel and two angle-error channels. A 10-kw UHF transmitter with a similar 85-ft reflector but with an azimuth-elevation mount is located several miles from the receiver. *Pioneer IV* was tracked using a one-way communication link consisting of a stable transmitter in the probe and the Goldstone receiver. In order to improve the doppler accuracy and provide a command link, future communications will be two-way, employing the transmitter and receiver at the tracking site and a transponder in the spacecraft. The transponder receives the transmitted wave from the DSN station and retransmits an exact multiple of the received carrier frequency for doppler measurements. Information is communicated to and from the spacecraft by modulation of the carrier. Hour angle, declination angle, and doppler shift are obtained from the Goldstone site.

For accurate orbit determination, it is necessary to obtain tracking data immediately after injection. Because of the low injection altitude (300 mi) and because of high angular tracking rates, the DSN stations are not able to track at all desired injection points. For this reason, the mobile station is located so as to observe the spacecraft near injection.

The mobile station is similar to the Puerto Rico Downrange Tracking Station used for tracking *Pioneer IV*. Since the mobile station is designed for relatively short-range communications (100,000 mi), its tracking equipment is somewhat simpler than that of the DSN stations. For example, the mobile station uses a 10-ft dish rather than an 85-ft reflector. Elevation angle, azimuth angle, and two-way doppler are obtained from the mobile station.

Although the computing center will rely primarily on the DSN and mobile station, it is expected that data will also be available from other radio tracking stations. Also, optical sightings (for example, from a Baker-Nunn satellite camera) can provide very accurate position fixes early in the trajectory by photographing the spacecraft against a star background. However, such observations are dependent on the weather, and the processing time may be inconveniently long.

C. Orbit-Determination Program

The radio tracking data are transmitted from the tracking stations to the computing center, where they are processed in the digital computer to determine the orbit of the spacecraft. The JPL tracking and orbit-determination program is described in detail in Ref. 2. Appendix D contains a derivation of some of the important equations used in the program. It will be noted that all of the computations are based on linear perturbation theory (Ref. 2). The required accuracy is attained by iterating on the linear solutions. Since a large amount of tracking data is obtained, some statistical estimation method must be used to obtain the best orbit from the redundant data. The program uses the maximum-likelihood method for estimating the values of the six parameters defining the coasting trajectory. The estimated values of the injection conditions are corrected by comparing predicted values of the radio tracking measurements with the actual observed values.

The program accepts angle data (azimuth and elevation or hour-angle and declination), range-rate data, and range data from a number of different stations. The computer corrects the input data for systematic errors, such as the refraction correction for angle data. It is assumed that each type of data is contaminated with gaussian noise, and that the noise is uncorrelated between stations and data types. The weighting of the different data types in determining the orbit can be adjusted according to engineering estimates of their accuracy. As explained in Appendix D, this weighting can also be used to take into account time correlation in each type of data. (When the effect of time correlation is approximated in this way, the method of maximum likelihood becomes equivalent to the method of least-square error.) The program will also solve for constant bias errors in each type of data, but it will be assumed here that the data are already corrected for bias errors, and thus, the noise has zero mean.

As shown in Appendix D, an intermediate step in the determination of the maximum-likelihood estimate of the injection conditions is the calculation of the noise moment matrix of injection conditions J^{-1}. The J^{-1} matrix can be used to answer many questions concerning the effects of radio tracking errors on the accuracy of mid-course guidance and the requirements on the tracking net. Specifically, the following problems can be studied:

(1) The quality of the estimates of miss components and injection errors as a function of tracking time after injection

(2) The required accuracy in measuring range rate and tracking angles to satisfy the mission requirements

15

(3) The desirability of measuring range and the required accuracy

(4) The relative contribution of different stations to the orbit determination, and thus, the effect of a station being inoperative due to equipment failure

(5) The effect of geographic location of a station on the accuracy of the orbit determination

(6) The accuracy of the predicted acquisition coordinates for different stations

(7) The re-establishment of the orbit after a mid-course maneuver and before a subsequent maneuver, such as an additional mid-course maneuver or a retro-maneuver.

The JPL orbit-determination program uses the following set of Earth-fixed injection parameters:

r = radius from center of Earth, meters

ϕ = latitude, deg

θ = longitude, deg

v = velocity in coordinate system rotating at Earth's rate, meters/sec

γ = angle of velocity vector above local horizontal plane, deg

σ = angle of projection of velocity vector on local horizontal plane measured from North, deg

Thus, the noise moment matrix of the uncertainties in the estimates of the six injection coordinates is (Eq. D-28, Appendix D)

$$J^{-1} = \begin{bmatrix} \sigma_r^2 & \rho_{r\phi}\sigma_r\sigma_\phi & \rho_{r\theta}\sigma_r\sigma_\theta & \rho_{rv}\sigma_r\sigma_v & \rho_{r\gamma}\sigma_r\sigma_\gamma & \rho_{r\sigma}\sigma_r\sigma_\sigma \\ & \sigma_\phi^2 & \rho_{\phi\theta}\sigma_\phi\sigma_\theta & \rho_{\phi v}\sigma_\phi\sigma_v & \rho_{\phi\gamma}\sigma_\phi\sigma_\gamma & \rho_{\phi\sigma}\sigma_\phi\sigma_\sigma \\ & & \sigma_\theta^2 & \rho_{\theta v}\sigma_\theta\sigma_v & \rho_{\theta\gamma}\sigma_\theta\sigma_\gamma & \rho_{\theta\sigma}\sigma_\theta\sigma_\sigma \\ & & & \sigma_v^2 & \rho_{v\gamma}\sigma_v\sigma_\gamma & \rho_{v\sigma}\sigma_v\sigma_\sigma \\ & & & & \sigma_\gamma^2 & \rho_{\gamma\sigma}\sigma_\gamma\sigma_\sigma \\ \text{symmetrical} & & & & & \sigma_\sigma^2 \end{bmatrix} \tag{44}$$

where

σ^2 = variance in the estimate of a certain initial condition

ρ = correlation coefficient between estimates of two initial conditions

It is useful to transform the J^{-1} matrix to other coordinates of more direct interest. Let

$$W' = \begin{bmatrix} \frac{\partial M_1}{\partial r} & \frac{\partial M_1}{\partial \phi} & \frac{\partial M_1}{\partial \theta} & \frac{\partial M_1}{\partial v} & \frac{\partial M_1}{\partial \gamma} & \frac{\partial M_1}{\partial \sigma} \\ \frac{\partial M_2}{\partial r} & \frac{\partial M_2}{\partial \phi} & \frac{\partial M_2}{\partial \theta} & \frac{\partial M_2}{\partial v} & \frac{\partial M_2}{\partial \gamma} & \frac{\partial M_2}{\partial \sigma} \end{bmatrix} \tag{45}$$

be the matrix of differential coefficients which transforms from injection perturbations to miss components M_1 and M_2 at the target. Then, the moment matrix of the uncertainties in miss components is

$$\begin{bmatrix} \overline{M_1^2} & \overline{M_1M_2} \\ \overline{M_1M_2} & \overline{M_2^2} \end{bmatrix} = \overline{W'\delta X_u (W'\delta X_u)^T} = W'J^{-1}W'^T \tag{46}$$

Setting the quadratic form equal to a constant k^2,

$$[M_1M_2]\,[W'J^{-1}W'^T]^{-1}\begin{bmatrix} M_1 \\ M_2 \end{bmatrix} = k^2 \tag{47}$$

gives the equation for equiprobability contours. These contours are ellipses which contain 100 $(1 - e^{-\frac{1}{2}k^2})$ per cent of all possible miss components. Often it is useful to find the semimajor axis λ and the semiminor axes of the dispersion ellipse, which is done by diagonalizing $W'J^{-1}W'^T$.

D. Accuracy of Tracking Data

In order to calculate the accuracy of orbit determination, it is necessary to make an estimate of the accuracy of the tracking data from the DSN stations and the mobile station. These estimates are used to weight the different types of data in computing the J^{-1} matrix. It is assumed that the tracking data are corrected for all predictable and measurable errors. An example of a predictable correction is that applied to tracking angles to compensate for the standard refraction of the atmosphere. A measurable error is one which can be determined by calibrating the equipment in various tests. An example of a measurable type of error is the misalignment between the mechanical and electrical axes of the radio telescope antenna, which can be determined by boresighting to beacons. After all predictable and measurable errors are removed, the remaining errors are random with zero mean. Only the random errors are considered in this Part. An example of a random error is the error in tracking angles due to thermal noise in the receiver, which causes jitter in the angle servos. With each random error, there is associated a correlation interval or noise period, which can be defined loosely as the smallest time interval over which two samples of the noise are essentially independent. For example, the angle jitter in the servos due to receiver noise is essentially independent over time intervals which exceed the dominant time constant of the angle servos.

It can be seen that each type of tracking data from each station can be contaminated by several independent noise sources. It is assumed that the noise from each source can be specified by an idealized autocorrelation function which has a value of σ^2 for $0 < t < \tau$ and is zero for $t > \tau$; σ^2 is the variance of the particular kind of noise,

and τ is the time interval over which the noise is correlated. In other words, it is assumed that the noise is perfectly correlated over any interval less than τ and uncorrelated over any interval greater than τ. In addition, it has been approximated that σ^2 does not vary with range. Table 2 shows the assumed characteristics of the noise in the data for the two types of stations.

Consider first the accuracy of the two-way doppler measurements. The doppler frequency is approximately

$$f_d = 2af_c\frac{v}{c} \tag{48}$$

where

f_d = doppler frequency, cps

f_c = frequency transmitted by tracking station, cps

v = component of spacecraft velocity away from tracking station, meters/sec

a = ratio of transmitted to received frequency in transponder

c = velocity of light, meters/sec

Substituting $a = 1, f_c = 960$ mc, and $c = 3 \times 10^8$ meters/sec in Eq. 48, it is seen that one doppler cycle corresponds to a velocity of 0.15 meters/sec. It is assumed that the doppler cycles are counted at the carrier frequency. If the doppler frequency is counted for n sec, a one-cycle roundoff error causes a random error of $1/n$ cps in f_d, and the corresponding velocity error is $0.15/n$ meters/sec. However, as n increases, the error due to neglecting derivatives of the spacecraft's acceleration also increases. It is estimated that the optimum duration for counting doppler cycles is about 1 sec. Another source of random error in doppler measurements is the unpredictable time variation of the refraction of the atmosphere and ionosphere. The effective path length for the radio waves depends on the index of refraction along the path in the atmosphere. A changing index of refraction causes a changing path length and, thus, produces a doppler shift which is interpreted as a change in spacecraft velocity. The changes in refraction are due to turbulence, changes in water vapor concentration, etc.

During the round-trip transit time of a particular wave train, the frequency of the transmitter may wander a small amount from its original value. This wander could be caused, for example, by a mechanical shock or a slight change in temperature of the frequency standard. The frequency drift will be erroneously interpreted as a doppler shift. It is estimated that all of these error sources will contribute an rms velocity error of 0.15 meters/sec, as shown in Table 2. The noise period is estimated to be less than 10 sec.

As shown in Table 2, there are three noise components which contribute to angle error. The main cause of servo jitter is equivalent thermal noise in the angle-error channels of the receiver. The thermal noise is due to random motion of electrons in the sensitive receiver and to energy radiated from the Earth and sky. This broad-band thermal noise is filtered by the angle servos, resulting in a noise period of several seconds. The magnitudes of σ and τ for this noise component are determined by direct measurement. Random variations in the refraction of the atmosphere and ionosphere cause noise in the angle measurements. This effect is analogous to the twinkling of visible stars. The value of σ is estimated to be 0.01 deg. These estimates of servo and refraction noise agree reasonably well with autocorrelation functions computed from 2-hr segments of actual tracking data (Ref. 7).

The very low-frequency noise component is due to structural deflections of the large tracking antenna. The antenna and supporting structure are subject to deformations from varying wind loads and temperatures. As the position of the reflector is changed, the structure is subjected to varying gravity loads. The bearings and structure undergo small inelastic deflections. The magnitudes of σ and τ for this type of error were estimated from measurements of boresight error taken at 6-hr intervals during a 6-day period. The length of τ is so great for this error that in some applications it would be regarded as a bias error. The weighting of the angle data in the J^{-1} matrix is determined largely by the low-frequency noise component, because of the very large value of τ.

Table 2. Assumed noise characteristics

Station type	Data type	Noise source	σ	τ, min
Deep Space Net	range rate, meters/sec	roundoff changing refraction frequency drift	0.15	<0.16
	declination, deg	servo jitter refraction antenna-structure deflections	0.03 0.01 0.01	<0.16 0.5 300
	hour angle, deg	same as declination		
Mobile (maximum range, 50,000 mi)	range rate, meters/sec	same as range rate for Deep Space Net		
	elevation angle, deg	servo jitter refraction antenna-structure deflections	0.1 0.01 0.1	<0.16 0.5 60
	azimuth angle, deg	same as elevation		

17

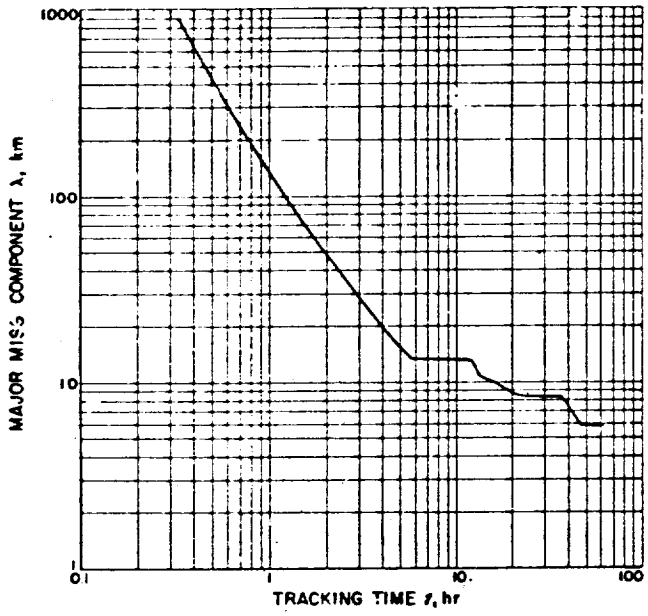

Figure 4. Miss at the Moon due to radio tracking errors

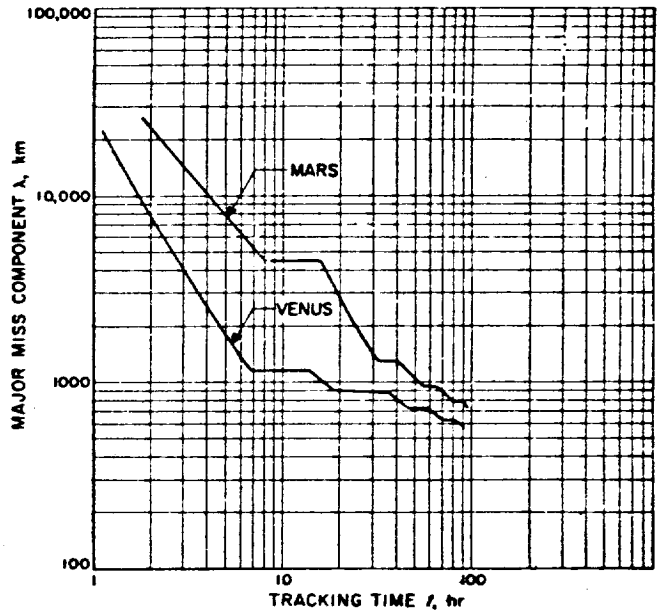

Figure 5. Miss at Venus and Mars due to radio tracking errors

E. Results

In order to answer some of the questions raised previously, J^{-1} matrices have been computed for a number of different tracking situations. These matrices have been computed using a digital-computer program, which is a modification of the existing orbit-determination program. The results from the modified program have been verified using a scatter-diagram approach with artificial tracking data.

The results for a lunar trajectory will be described first. The spacecraft is injected over the South Atlantic Ocean near Ascension Island. The spacecraft impacts the Moon 66 hr after injection. It is assumed that while the spacecraft is on this trajectory, it is tracked by the mobile station at Johannesburg, South Africa, and by the DSN station at Goldstone. The characteristics of the data from these stations are listed in Table 2. It is assumed that each type of data is sampled once every 10 sec. Figure 4 shows the uncertainty in the miss at the Moon due to radio tracking errors. The abscissa t is tracking time measured from injection. The ordinate λ is the length of the semi-major axis of the 40 per cent probability ellipse of miss components at lunar impact. In Fig. 4, the mobile station tracks from shortly after injection until the spacecraft goes out of range at $t = 5.5$ hr. The data from the mobile station reduce λ to 13 km. Goldstone acquires the spacecraft at $t = 12$ hr, and data obtained during the first pass reduce λ to 8.2 km. If a mid-course maneuver is made at some time $t = t_g$, the radio tracking errors will contribute an error $\lambda(t_g)$ to the over-all miss at the target. It can be seen from Fig. 4 that the earlier the correction is applied, the larger the tracking error.

Figure 5 shows the uncertainty in the miss at Venus and Mars due to radio tracking errors. The transit times on these trajectories are 108 days for Venus and 177 days for Mars. The curves in Fig. 5 are not drawn beyond 100 hr since the mid-course maneuver would normally be made within the first few days. On the Venus trajectory, the spacecraft is tracked from the mobile station and from the DSN station at Goldstone for roughly the same time periods as in the lunar case. However, the results for the Mars trajectory are somewhat unrealistic in that the orbit is determined entirely from Goldstone data. There is no tracking from the mobile station, since the spacecraft does not come above the horizon at South Africa until it exceeds the maximum range of the mobile station. Actually, for this trajectory, it would be necessary to relocate the mobile station (in Australia, for example) in order to obtain early tracking data to predict Goldstone acquisition coordinates. Of course, the added data would also improve λ.

In Fig. 4 and 5, if the angle data from both stations are omitted, there is a negligible degradation in the accuracy of orbit determination. The relative accuracy of the doppler and angle data is such that the orbit is determined almost entirely from the doppler data. If the angle data are retained and the σ in the range-rate data from both stations is increased from 0.15 meter/sec to 1 meter/sec,

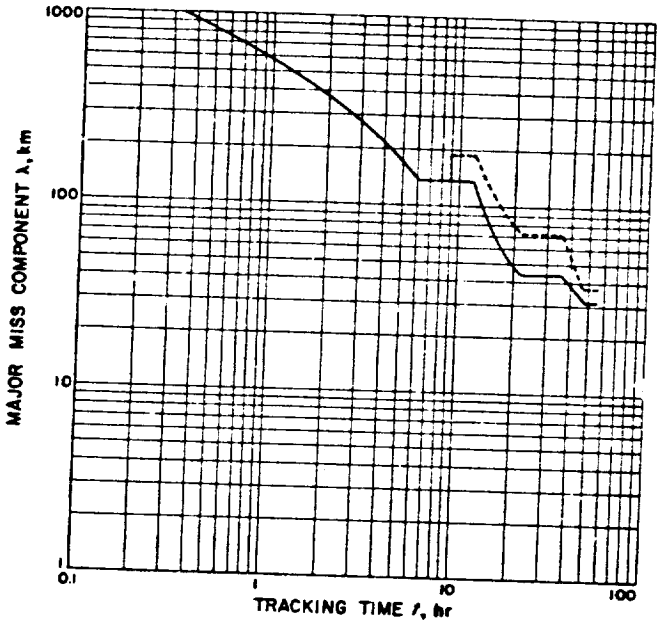

Figure 6. Accuracy of orbit determination with mid-course maneuver

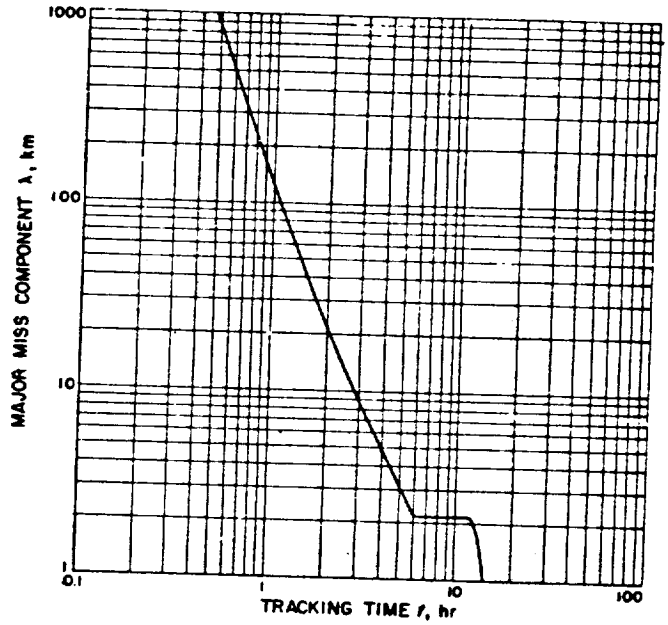

Figure 7. Accuracy of orbit determination with range data

$\lambda(20)$ is increased by a factor of about 3.5 for all three cases. It has been observed in a number of cases that for accurate orbit determination it is necessary to obtain tracking data near injection. The data acquired in just a few minutes at this time have a very powerful effect in reducing λ. If no data are obtained until several hours after injection, λ may be quite large.

The solid curve in Fig. 6 shows $\lambda(t)$ for a different lunar trajectory. The spacecraft is injected over Ascension Island as in the previous case. The spacecraft's closest approach to the surface of the Moon (300 mi) occurs 51 hr after injection. In this case, it is assumed that the range-rate data from both stations have an accuracy σ of 1 meter/sec. The dashed curve in Fig. 6 shows $\lambda(t)$ when there is a mid-course maneuver. It is assumed that the mid-course maneuver is made at $t_g = 9$ hr, although this is not the optimum time. Because of pointing and shutoff errors in the mid-course guidance system, there will be some uncertainty in the direction and magnitude of the velocity vector applied to the spacecraft. Using typical values for these uncertainties, the orbit determination degenerates at t_g, as shown by the dashed curve in Fig. 6. Subsequent tracking reduces λ considerably. It may be necessary to redetermine the orbit quite accurately after a mid-course maneuver in order to calculate the impulse for a retro-maneuver or as part of a scientific experiment.

Figure 7 shows the effect on the solid curve of Fig. 6 when range data from both stations are utilized in addition to angle and range-rate data. It is assumed for the range data that $\sigma = 10$ meters and $\tau < 0.16$ min. It can be seen that range data are very useful in determining orbits. Curves similar to those of Fig. 4 through 7 can be plotted for quantities other than λ. For example, the standard deviation in injection conditions (the square root of the diagonal elements of the J^{-1} matrix) can be plotted as a function of tracking time; or the J^{-1} matrix can be transformed to other coordinates, such as uncertainties in time of flight, velocity components at the target, etc.

F. Further Results

Figure 8 shows how the accuracy of orbit determination on the 51-hr trajectory varies with the magnitude of the noise on the range-rate data. The ordinate of the graph is $\lambda(20)$ and the abscissa is the value of σ for the range-rate data, $\sigma_{\dot{r}}$. The value of λ at 20 hr is chosen because considerations of fuel economy and component error indicate that the optimum t_g is between 15 and 20 hr for this trajectory. It is assumed that $\sigma_{\dot{r}}$ is the same for both stations and that $T < 0.16$ min. The noise in the angle data is the same as that in Table 2. Note that in Fig. 8, when $\sigma_{\dot{r}} = 1$ meter/sec, $\lambda(20) = 49$ km, which agrees with the solid curve in Fig. 6. As $\sigma_{\dot{r}}$ becomes larger in Fig. 8, the range data contribute less to the over-all orbit determination. The curve approaches an asymptote $\lambda(20) = 1100$ km, which is the value of $\lambda(20)$ if only angle data are used.

19 19

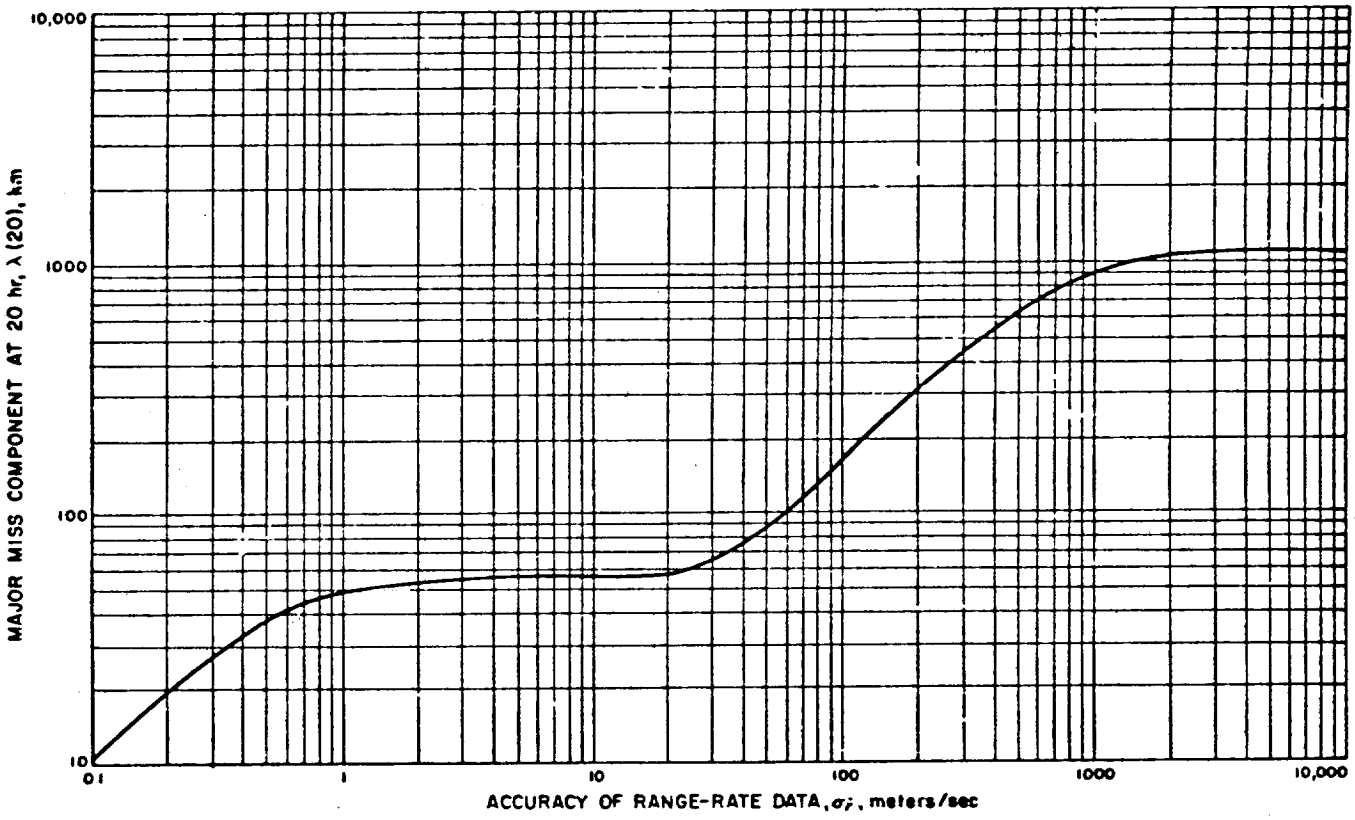

Figure 8. Effect of range-rate accuracy on major miss component

Figure 9 shows the effect of varying the accuracy of the angle data from each station. The value of σ for the low-frequency component of noise in hour angle and declination is σ_α and σ_λ is the value of σ for the low-frequency component of noise in elevation and azimuth. The curves approach a lower asymptote because of the other components of angle noise in Table 2. In Fig. 9, it is assumed that $\sigma_{\dot{r}} = 1$ meter/sec. If $\sigma_{\dot{r}} = 0.15$ meter/sec had been used, the curves would approach the upper asymptote for even smaller values of σ_α and σ_λ.

It is instructive to consider how the accuracy of orbit determination is affected by the quantity of tracking data. Figure 10 shows the uncertainty in the miss at the Moon on the 51-hr trajectory as a function of the number of radio tracking measurements. The ordinate λ is evaluated at t_p, which is assumed to be 20 hr after injection. The abscissa n is the total number of radio tracking measurements taken in the 20-hr period. A measurement is any one observation of doppler frequency or a tracking angle. Since the total tracking time is constant, n is varied by changing the interval between measurements.

Curve A of Fig. 10 shows $\lambda(20)$ when the orbit is determined using all of the types of data listed in Table 2.

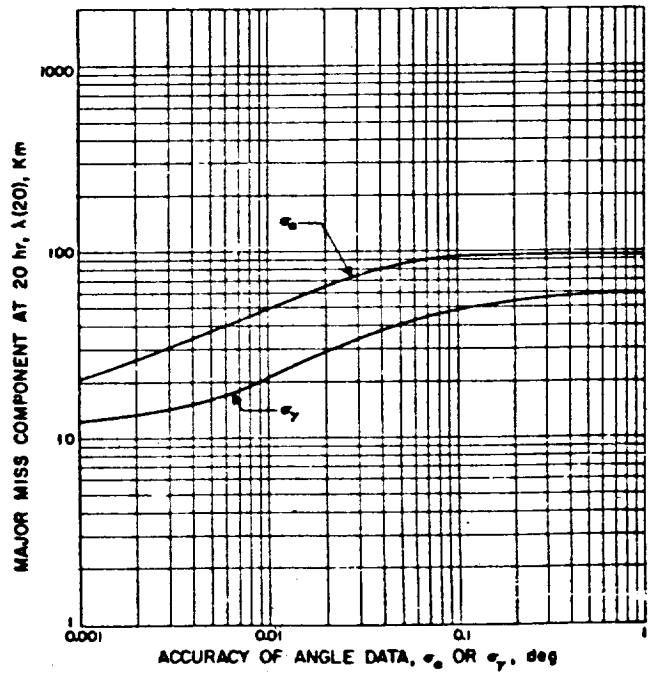

Figure 9. Effect of angle accuracy on major miss component

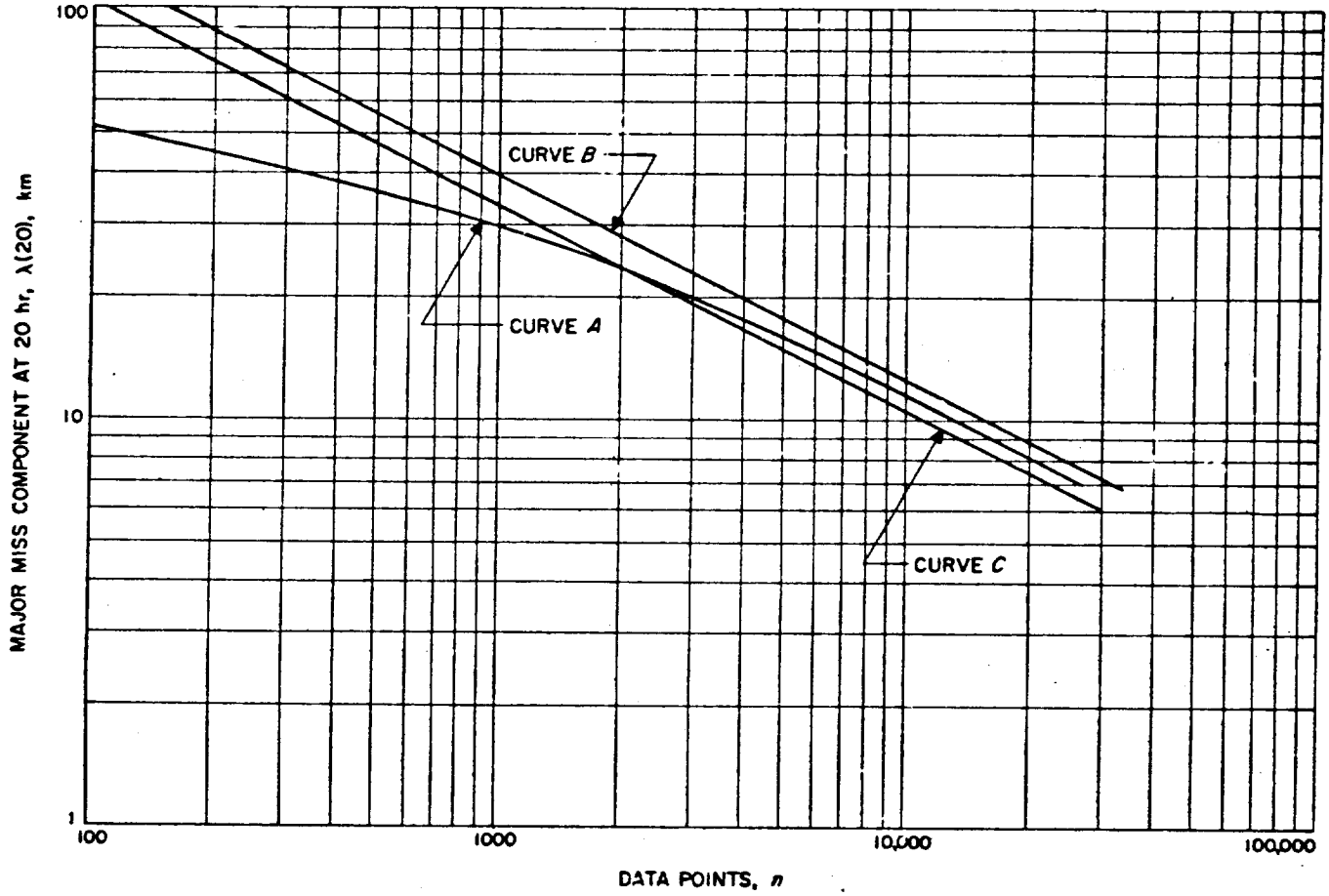

Figure 10. Miss at the Moon due to radio tracking errors as a function of total number of measurements

It can be seen from Table 2 that the noise contaminating the angle data consists of two relatively high-frequency components and one very low-frequency component. It is assumed here that the angle data will be smoothed somewhat before being used in the orbit-determination program. This will eliminate the high-frequency components, leaving only the very low-frequency noise. It is useless to sample the smoothed angle data too frequently, because the measurements will not be independent. It is estimated that all of the useful angle information can be extracted from 20 samples of the smoothed angle data taken at equal intervals over the tracking time. Therefore, for curve A, n consists of 20 angle measurements; all the rest are doppler measurements. If a doppler measurement is taken every 10 sec when the spacecraft is visible from Johannesburg or Goldstone, the total number of data points is $n = 4400$. It should be noted that as n becomes large, curve A approaches an asymptote with a slope of $-\frac{1}{2}$. Thus, for large n, $\lambda(20)$ is proportional to $1/\sqrt{n}$. This is to be expected, since $\lambda(20)$ is analogous to the standard deviation of the sample mean.

Curve B shows $\lambda(20)$ vs n when the orbit is determined entirely from range-rate data. It is assumed that the data are sampled at equal time intervals whenever the spacecraft is visible from a station, the time intervals being inversely proportional to n. Curve B is a straight line, with slope $-\frac{1}{2}$ over the whole range of n-values shown in Fig. 10. If curve B were extended to smaller values of n, however, it would deviate from the straight line.

Comparison of curves A and B shows that, for small n, the use of angle data causes a considerable improvement in $\lambda(20)$. However, for the assumed doppler accuracy and for large n, only slight improvement in $\lambda(20)$ results. Before drawing any general conclusions concerning angle data, it should be remembered that Fig. 10 is drawn for a particular trajectory. It is possible that the tracking geometry in certain special cases could result in a requirement for angle data in order to resolve ambiguities in the

21

doppler data and insure rapid convergence of the orbit-determination program.

For curves *A* and *B*, it was assumed that the observations were taken at equally spaced time intervals. Let $r(t)$ be the range rate from a station as a function of time. It has been observed that a small change in the orbit will produce a large change in the functional form of $r(t)$ during the first part of flight. This suggests that it may be more efficient to vary the interval between observations rather than taking observations at constant intervals. Curve *C* uses only doppler data, as did curve B. However, in curve *C*, the data were sampled at a rate which decreased with increasing time. Comparison of curves *B* and *C* shows that the tapered sampling rate results in a smaller $\lambda(20)$ for the same total number of data points (n).

It might be expected from Fig. 10 that the accuracy can be improved without limit by increasing n. Such a conclusion is invalid if all factors are taken into account. The curves continue to decrease only if the contaminating noise is random with zero mean. This means that the data must be corrected for all systematic and bias errors. Obviously, it is impractical to correct for all of these errors, and a point will be reached where neglected systematic and bias errors will limit the accuracy instead of the random errors. Also, it has been assumed that the range-rate data are uncorrelated in time. Actually, there may be some small noise component in the range-rate data which is correlated over a finite time interval. For example, turbulence in the atmosphere can cause local variations in the index of refraction which, in turn, cause variations in the effective path length for the radiation. The changing path length produces correlated noise in the range-rate measurements. Thus, when n becomes very large, the samples of range-rate data will no longer be independent and $\lambda(20)$ will stop decreasing.

There are other practical reasons for limiting the value of n. If too many data points are used, the computing time required for a fit may become inconveniently long. It is estimated that three iterations using 4400 data points at each iteration require 3 hr on the IBM 704 digital computer. On the pass in which the maneuver is to be made, adequate time must be allowed to acquire additional tracking data, compute the orbit and correction, transmit the commands, and observe the maneuver. It is conceivable that the limited precision of computation may cause the least-square fit to deteriorate if a very large number of data points is used. However, investigations show that this effect is negligible up to 8000 data points.

For the interplanetary trajectories, an additional source of error is the uncertainty in the Astronomical Unit (AU–a unit of length equal to the mean radius of the Earth's orbit used for measuring distances in the solar system). In the ephemeris, the positions of the planets are tabulated quite accurately in terms of AU. However, at the present time there is an uncertainty of the order of one part in 2000 in the conversion factor from AU to ordinary length units such as meters. This results in an uncertainty of 21,000 km in the miss at Venus and an uncertainty of 25,000 km in the miss at Mars when the orbit is computed from heliocentric injection conditions expressed in ordinary length units. Note that this miss is not a random variable but rather the upper limit of an unknown constant. However, it is anticipated that the uncertainty in the AU will be reduced in the near future by tracking of space probes and radar-ranging to planets. Although there are corresponding uncertainties in the physical constants of the Earth–Moon system which would affect the accuracy of lunar trajectories, it is believed that these constants will soon be known accurately enough so that they contribute an error which is negligible compared to other errors.

IV. GUIDANCE SYSTEMS

Returning to the subject of mid-course maneuvers, as distinct from orbit determination, possible schemes of mechanization are summarized in Table 3.

Scheme 1 (Ref. 8) is especially suited to spinning payloads since, in addition to providing the method of thrust vector control, the spin provides a direction fixed in space. However, it is found that to avoid excessive amounts of propellant, the first of the two maneuvers must be made shortly after injection (e.g., 1 to 2 hr on a lunar trajectory). The orbit would not usually be determined sufficiently

Table 3. Possible mid-course guidance systems

Scheme	Terminal coordinates controlled	Impulse	Constraints on rocket orientation
1	Two miss components	Variable (twice)	Fixed direction
2	Two miss components	Variable	Restricted to a plane
3	Two miss components	Fixed	None
4	Two miss components and either speed or time of arrival	Variable	None

22

by radar-tracking at that time, and also, the spacecraft may not be visible from the tracking site which has the command capability. In the early stages of the NASA space program, only the Goldstone site will have the command capability, and spacecraft injected over the South Atlantic Ocean are not visible from that site until about 11 hours after injection (Fig. 9).

In scheme 2 of Table 3, it was shown that both miss components can be controlled when the rocket impulse is restricted to a plane. For a given point on a given trajectory, one plane exists (the critical plane) for which the maneuver is a minimum; however, the impulse need not be applied in that plane. In practice it may be convenient to restrict the maneuver to the plane perpendicular to the Sun–probe line or the Earth–probe line. Thus, if the rocket is mounted to fire perpendicularly to the Sun–probe line, then, in orienting the spacecraft and rocket for the maneuver, one face of the craft (e.g., the face carrying solar panels) is never turned away from the Sun.

If the spacecraft and rocket could be oriented in any desired manner, then scheme 2 (in the critical plane) or scheme 4 would be employed. The authors have concentrated most of their attention on these schemes. Scheme 4 permits the greatest flexibility, since speed or time of arrival may also be controlled. Subsequent discussions refer to schemes 2 or 4 of Table 3 for a rocket mounted rigidly in a spacecraft which can be pointed in any desired direction by command from the ground.

Except when the mid-course rocket is developing thrust, attitude control of the spacecraft may be accomplished with a system of gas jets for lunar missions; but for longer interplanetary missions, the addition of flywheel control would be desirable. Provided the electrical power comes from solar panels, the weight of a flywheel system does not increase with journey time. Further discussion of such attitude-control systems is, however, beyond the scope of this report.

The ease of shutting off and restarting liquid-propellant rocket motors makes them attractive for mid-course maneuvers. Thrust levels can be quite low (50 lb), and the lower specific impulses of monopropellants are acceptable in simplifying the propulsion unit. A separate tighter form of attitude stabilization would, however, be required during burning of the rocket, e.g., gimbaling the rocket motor. Shutoff of the motor would be dependent upon the integrated output of an accelerometer, mounted with the sensitive axis parallel to that of the thrust vector.

Apart from tracking considerations (Part III), the choice of T (the time of application of the maneuver) is influenced by the magnitude of the correction as a function of T, and the effect of errors in applying the maneuver (e.g., in pointing the rocket). The calculation of the magnitude of the maneuver was presented in II-D, the result being dependent on the relative values and cross-correlations of the injection errors. However, it is interesting to note in Fig. 11, where the mid-course maneuver to correct one-at-a-time injection errors is plotted against T for a lunar impact trajectory, that whereas some injection errors should be corrected as early as possible, the optimum time for correcting other errors is some time after injection. It follows that the optimum maneuver point depends on the particular injection-guidance system.

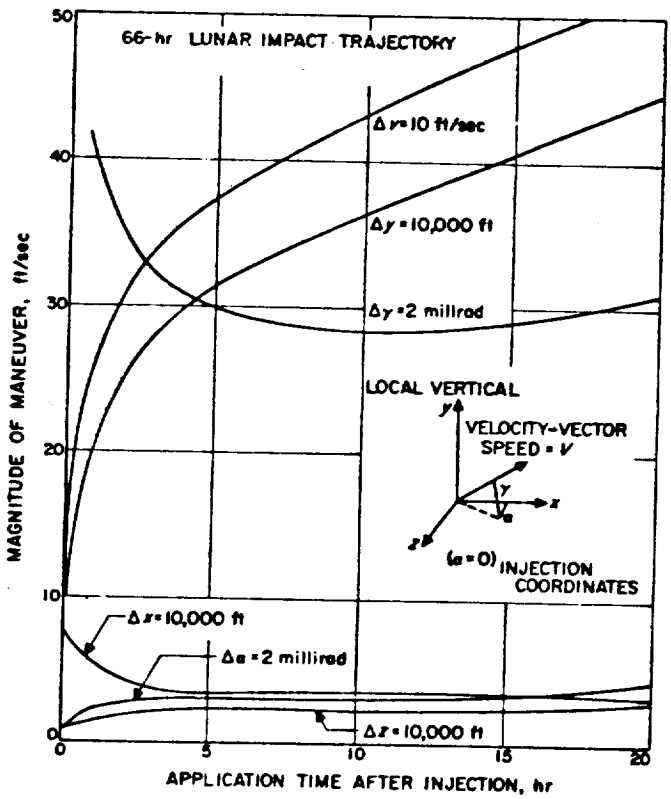

Figure 11. Mid-course maneuver to correct injection errors

By way of illustration, the rms magnitude of the mid-course maneuver is plotted against T in Fig. 12 (for the *Agena* guidance system as used for *Discoverer* missions). The calculations for this graph employed the statistical procedures presented in Fig. 2. The graph shows two curves: One refers to the correction of miss components only and the other to the correction of miss components and flight time. In the event that only miss components are corrected, the corresponding variations in lunar impact speed and flight time are given in Fig. 13 (calculated by Eq. 43).

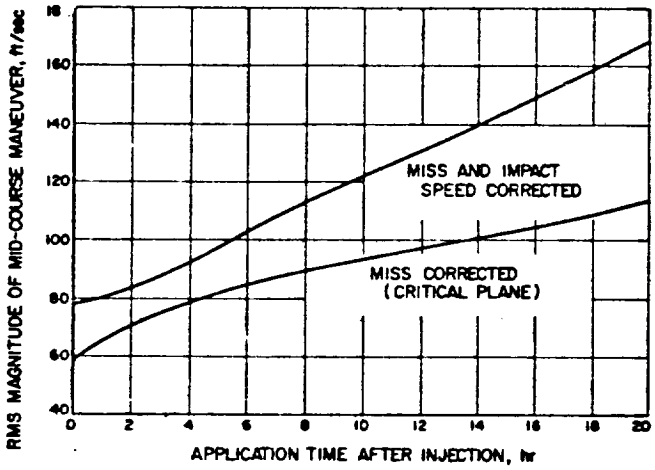

Figure 12. Mid-course maneuver for the *Agena–Discoverer* guidance system

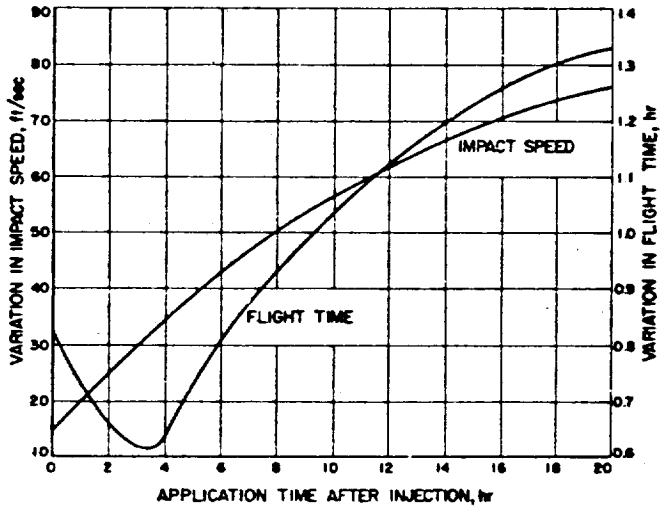

Figure 13. Variation of flight time and impact speed when only miss components are corrected by a maneuver in the critical plane (trajectory and guidance as in Fig. 12)

In estimating the effects of errors in applying the maneuver, the authors have, in the final analysis, resorted to evaluating upper bounds of the errors (from Eq. 30). However, in preliminary studies it is much more convenient to use the approximate formulas derived in II-E. Statistically averaged coefficients were deduced which relate errors in the direction and magnitude of the maneuver to miss at the destination. These coefficients are plotted in Fig. 14 and 15 against application time of the maneuver for a 66-hr lunar-impact trajectory. The maneuver implied would be to correct miss components and speed at the Moon. Fig. 14 shows the coefficient λ of Eq. 34 expressed in two different sets of units for convenience of interpretation, it being the factor for errors in magnitude or direction. Fig. 15 shows the coefficients μ_v, μ_ζ, and μ_η of Eq. 36 for estimating the terminal speed errors, the mid-course maneuver being one which controls speed at the destination.

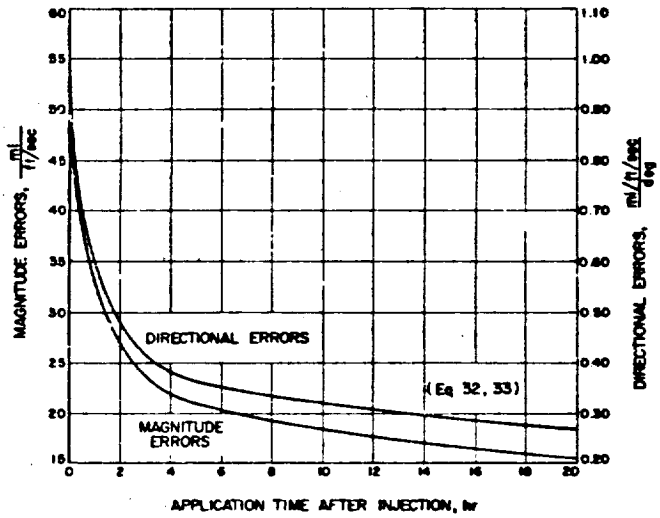

Figure 14. Coefficients relating miss at the Moon to errors in magnitude and direction of mid-course maneuver

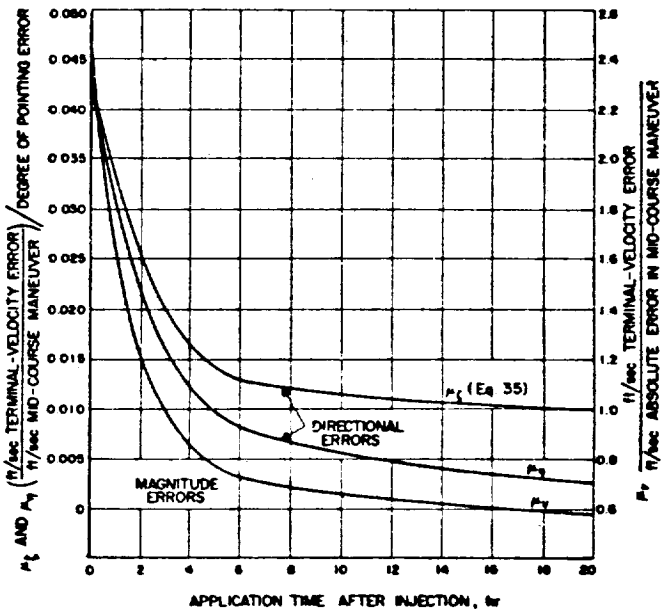

Figure 15. Coefficients relating speed at the Moon to errors in magnitude and direction of mid-course maneuver

V. CONCLUSIONS

Radio-command mid-course guidance is regarded as having great potential for future lunar and interplanetary missions. It is suitable for ensuring impact on a small, preselected area of the surface of the Moon for guidance prior to the creation of a lunar satellite, and for sending a recoverable space probe around the Moon and back to Earth. Futhermore, provided the measure of the Astronomical Unit is improved, such guidance will ensure approaches within 10,000 mi of the planets Mars and Venus.

Examination of Fig. 11 through 14 reveals that unless the mancuver is made within the first hour after injection (and this would not usually be possible) the choice of the maneuver point is not critical. It can be made within the first 100,000 mi of a lunar flight or the first few million miles of an interplanetary flight.

It is perhaps instructive to quote estimates of the accuracy that might be achieved with a single-impulse, radio-command, mid-course guidance system. Illustrative results are presented in Table 4.

Table 4. Representative figures for the accuracy of mid-course guidance (rms quotations of errors)*

Destination	Orbit determination miss, mi	Coefficient mi/ft/sec	Assumed error ft/sec	Miss mi	Coefficient mi/deg	Assumed error deg	Miss mi	Total miss mi
Moon	7	22	1	22	38	0.5	19	30
Mars	1500*	3570	1	3570	6230	0.5	3115	5000
Venus	700*	1970	1	1970	3430	0.5	1715	2700

*Correction in the critical plane for miss components only.
*It is assumed that the uncertainty in the Astronomical Unit will be reduced in the near future by more than one order of magnitude (Ref. 9). Otherwise, the miss at Mars and Venus would be of the order of 15,000 mi (for 1 in 2000).

APPENDIX A

Correcting Velocity Components

The coordinates x_2, y_2 and z_2 on a ballistic trajectory at any time t_2 are functions of the coordinates x_1, y_1, z_1, $\dot{x}_1$, $\dot{y}_1$, and $\dot{z}_1$ at any previous time t_1. Hence, by taking only the first-order terms of a generalized Taylor expansion,

$$\delta x_2 = \frac{\partial x_2}{\partial x_1}\delta x_1 + \frac{\partial x_2}{\partial y_1}\delta y_1 + \frac{\partial x_2}{\partial z_1}\delta z_1 + \frac{\partial x_2}{\partial \dot{x}_1}\delta \dot{x}_1 + \frac{\partial x_2}{\partial \dot{y}_1}\delta \dot{y}_1 + \frac{\partial x_2}{\partial \dot{z}_1}\delta \dot{z}_1 \qquad \text{(A-1)}$$

and, similarly, for δy_2 and δz_2, where the perturbations are to be interpreted as coordinate variations from a standard trajectory. In addition to the six coordinate perturbations at time t_1, let a further perturbation be added in the form of an impulse of velocity with components V_x, V_y, and V_z, such that

$$\delta x_2 = -\frac{\partial x_2}{\partial \dot{x}_1}V_x - \frac{\partial x_2}{\partial \dot{y}_1}V_y - \frac{\partial x_2}{\partial \dot{z}_1}V_z \qquad \text{(A-2)}$$

and, similarly, for δy_2 and δz_2. The net result will then be that $\delta x_2 = \delta y_2 = \delta z_2 = 0$, since the applied velocity perturbation will exactly cancel the effects of the six coordinate variations at time t_1. Equation 1 is a statement of this result in matrix notation.

25 25

APPENDIX B

Minimization of the Magnitude of the Maneuver

Equation 4, written out in full, is

$$\begin{aligned} -M_1 &= k_{11}V_x + k_{12}V_y + k_{13}V_z \\ -M_2 &= k_{21}V_x + k_{22}V_y + k_{23}V_z \end{aligned} \tag{B-1}$$

where V_x, V_y, and V_z are to be chosen to minimize

$$V_x^2 + V_y^2 + V_z^2$$

subject to the two equations. The problem is solved by analogy with the problem in three-dimensional geometry of calculating the vector (drawn from the origin) perpendicular to the line of intersection of the two planes defined in Eq. B-1, regarding the velocity components as rectangular coordinates.

The normals to the two planes of Eq. B-1 have direction cosines proportional to k_{11}, k_{12}, k_{13} and k_{21}, k_{22}, k_{23}, respectively. The line of intersection of the two planes has direction cosines proportional to

$$(ik_{11} + jk_{12} + kk_{13}) \times (ik_{21} + jk_{22} + kk_{23}) \tag{B-2}$$

and the vectors iV_x, jV_y, and kV_z, the magnitude of which is a minimum, must be perpendicular to the vector of Eq. B-2. Hence,

$$\begin{aligned} (iV_x + jV_y + kV_z) \cdot [(ik_{11} + jk_{12} + kk_{13}) \\ \times (ik_{21} + jk_{22} + kk_{23})] = 0 \end{aligned} \tag{B-3}$$

The scalar triple product of Eq. B-3 can be written

$$\begin{vmatrix} k_{11} & k_{12} & k_{13} \\ k_{21} & k_{22} & k_{23} \\ V_x & V_y & V_z \end{vmatrix} = 0 \tag{B-4}$$

or

$$K_{21}V_x + K_{22}V_y + K_{23}V_z = 0 \tag{B-5}$$

where K_{ij} is the cofactor of the element k_{ij}.

APPENDIX C

Probability-Density Function of the Magnitude of the Mid-Course Maneuver

If the fundamental error sources during boost guidance are gaussian, then the six injection errors satisfy a six-dimensional gaussian distribution, and the velocity components u_1 and u_2 of II-D satisfy a two-dimensional distribution (Ref. 4).

Let

$$\begin{bmatrix} \overline{u_1^2} & \overline{u_1u_2} \\ \overline{u_2u_1} & \overline{u_2^2} \end{bmatrix} = \begin{bmatrix} a & b \\ b & b \end{bmatrix} \tag{C-1}$$

Then the probability of the velocity components being between u_1 and $u_1 + du_1$, and u_2 and $u_2 + du_2$ is

$$P_r = \frac{du_1 du_2}{2\pi\sqrt{ab - b^2}} \exp\left\{\frac{-1}{2}\begin{bmatrix} u_1 & u_2 \end{bmatrix}\begin{bmatrix} a & b \\ b & b \end{bmatrix}^{-1}\begin{bmatrix} u_1 \\ u_2 \end{bmatrix}\right\} \tag{C-2}$$

By an appropriate rotation of the u_1, u_2 axes, the moment matrix may be diagonalized, such that

$$P_r = \frac{du_1' du_2'}{2\pi\lambda_1\lambda_2} \exp\left(\frac{-u_1'^2}{2\lambda_1^2} - \frac{u_2'^2}{2\lambda_2^2}\right) \tag{C-3}$$

where

$$\begin{aligned} \lambda_1^2 &= \tfrac{1}{2}(a+b) + \sqrt{\left(\frac{a-b}{2}\right)^2 + b^2} \\ \lambda_2^2 &= \tfrac{1}{2}(a+b) - \sqrt{\left(\frac{a-b}{2}\right)^2 + b^2} \end{aligned} \tag{C-4}$$

Now let

$$\left.\begin{aligned} u_1' &= u\cos\theta \\ u_2' &= u\sin\theta \end{aligned}\right\}$$

Then

$$P_r = \frac{u\,du\,d\theta}{2\pi\lambda_1\lambda_2} \exp\left[-\frac{u^2}{2}\left(\frac{\cos^2\theta}{\lambda_1^2} + \frac{\sin^2\theta}{\lambda_2^2}\right)\right] \tag{C-5}$$

and the probability of the maneuver being between u and $u + du$ is

$$P_u = \int_0^{2\pi} P_r\,d\theta = \frac{u\,du}{2\pi\lambda_1\lambda_2}\int_0^{2\pi} \exp\left[-\frac{u^2}{2}\left(\frac{\cos^2\theta}{\lambda_1^2} + \frac{\sin^2\theta}{\lambda_2^2}\right)\right] d\theta \tag{C-6}$$

$$= \frac{u\,du}{2\pi\lambda_1\lambda_2} \exp\left[-\frac{u^2}{4}(\lambda_1^{-2} + \lambda_2^{-2})\right] \int_0^{2\pi} \exp\left[\frac{u^2}{4}(\lambda_2^{-2} - \lambda_1^{-2})\cos 2\theta\right] d\theta \tag{C-7}$$

$$= \frac{u\,du}{2\pi\lambda_1\lambda_2} \exp\left[-\frac{u^2}{4}(\lambda_1^{-2} + \lambda_2^{-2})\right] \int_0^{2\pi} \exp(x\cos\phi)\,d\phi \tag{C-8}$$

where

$$x = \frac{u^2}{4}(\lambda_2^{-2} - \lambda_1^{-2}) \tag{C-9}$$

and

$$\phi = 2\theta$$

The integral in Eq. C-8 is a Bessel function which is tabulated (Ref. 10)

$$P_u = \frac{u\,du}{\lambda_1\lambda_2} \exp\left[-\frac{u^2}{4}(\lambda_1^{-2} + \lambda_2^{-2})\right] J_0(ix) \quad \text{(C-10)}$$

For convenience, substitute

$$\psi = \frac{u}{\sqrt{\lambda_1\lambda_2}}$$
$$n = \frac{\lambda_1}{\lambda_2} \quad (n > 1) \quad \text{(C-11)}$$

n being the ratio of the major to minor axis of the dispersion ellipse in the u_1, u_2 plane.

The probability-density function is then:

$$\psi d\psi \exp\left[-\frac{\psi^2}{4}(n + n^{-1})\right] J_0(ix) \quad \text{(C-12)}$$

where

$$x = \frac{\psi^2}{4}(n - n^{-1})$$

This function is plotted in Fig. C-1 for three different values of n. The mean-square maneuver is

$$\overline{u^2} = \lambda_1\lambda_2 \int_0^\infty \psi^3 \exp\left[-\frac{\psi^2}{4}(n + n^{-1})\right] J_0(ix)\, d\psi \quad \text{(C-13)}$$

Let u_1 be the maneuver which includes 99 per cent of all cases. Then,

$$0.01 = \int_{u_1/\sqrt{\lambda_1\lambda_2}}^\infty \psi \exp\left[-\frac{\psi^2}{4}(n + n^{-1})\right] J_0(ix)\, d\psi \quad \text{(C-14)}$$

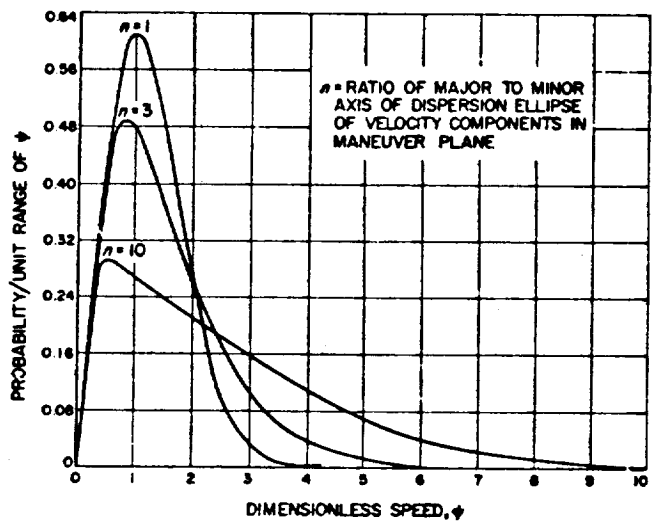

Figure C-1. Probability-density functions of the magnitude of a mid-course maneuver when restricted to a plane

By evaluating numerically[C-1] the integrals (C-13) and (C-14), the ratio

$$n = \frac{u_1}{\sqrt{\overline{u^2}}} \quad \text{(C-15)}$$

has been calculated for three different values of N (Table 1).

APPENDIX D

Computation of the Orbit From Radio Tracking Data

The coasting orbit is completely specified by the injection time and six injection parameters. The six injection parameters are denoted by X_j, where $j = 1, 2, \ldots 6$. One possible set of injection parameters was defined in III-C. Since the orbit is completely specified by the X_js, so is any observation of the orbit by an Earth-based radio tracking station. Let ψ be any one measurement along the orbit (e.g., range rate from a certain station). Then,

$$\psi_i = f_i(X_1, X_2 \cdots X_6; t) \quad \text{(D-1)}$$

where t is the time of observation. By the Taylor expansion, neglecting second- and higher-order terms,

$$\psi_i = f_i(X_{1S}, X_{2S} \cdots X_{6S}; t) + \sum_{j=1}^{6} \left.\frac{\partial f_i}{\partial X_j}\right|_{X_{jS}} \delta X_j \quad \text{(D-2)}$$

where the subscript S refers to the value on the standard trajectory and $\delta X_j = X_j - X_{jS}$ is the perturbation in the injection conditions. From Eq. D-2,

$$\delta\psi_i = \psi_i - \psi_{iS} = \sum_{j=1}^{6} \left.\frac{\partial f_i}{\partial X_j}\right|_{X_{jS}} \delta X_j \quad \text{(D-3)}$$

Equation D-3 is rewritten, using matrix notation

$$\delta\psi_i = U_i\, \delta X \quad \text{(D-4)}$$

[C-1] $\lim_{x\to\infty} J_0(ix) = \frac{e^x}{\sqrt{2\pi x}}$

27 27

where

$$U_i = \left[\left.\frac{\partial f_i}{\partial \zeta_1}\right|_{x_{st}} \cdots \left.\frac{\partial f_i}{\partial X_6}\right|_{x_{st}} \right] \tag{D-5}$$

and

$$\delta X = \begin{bmatrix} \delta X_1 \\ \delta X_2 \\ \delta X_3 \\ \delta X_4 \\ \delta X_5 \\ \delta X_6 \end{bmatrix} \tag{D-6}$$

Note that U_i is evaluated at the time when the ith observation is made.

The use of linear perturbation theory is justified for approximate calculations, because the injection guidance is accurate enough to inject the spacecraft on a coasting orbit which is close to the standard trajectory. Where extreme accuracy is required, linear perturbation theory can be used to obtain successive approximations for an exact iterative solution.

Now, let $\delta\psi$ be a column vector of all measurements of any type of data from any station. Suppose that the total number of measurements is m and, therefore, $i = 1, 2, \ldots m$. Equation D-4 becomes:

$$\delta\psi = U\delta X \tag{D-7}$$

where $\delta\psi$ is now an $m \times 1$ column vector and U is now an $m \times 6$ matrix of differential coefficients. Vector $\delta\psi$ represents the coordinates that would be measured by perfect instruments. Actually, the measurements are contaminated by noise, and the coordinates $\delta\xi$ are observed where

$$\delta\xi = \delta\psi + N \tag{D-8}$$

where

$$N = \begin{bmatrix} N_1 \\ N_2 \\ \cdot \\ \cdot \\ \cdot \\ N_m \end{bmatrix} \tag{D-9}$$

N being the noise component on each measurement. It is assumed that ξ is corrected for all systematic and bias errors.

It is also assumed that these noise components are associated with a multivariate gaussian distribution with probability-density function.

$$p(N) = \frac{1}{\sqrt{(2\pi)^m |K|}} \exp\left(-\tfrac{1}{2} N^T K^{-1} N\right) \tag{D-10}$$

where K is the noise moment matrix of all m measurement errors. Substituting Eq. D-8 into D-10,

$$p(N) = \frac{1}{\sqrt{(2\pi)^m |K|}} \exp\left[-\tfrac{1}{2} (\delta\xi - \delta\psi)^T K^{-1} (\delta\xi - \delta\psi)\right] \tag{D-11}$$

Computation of δX by the method of maximum likelihood (Ref. 11) consists of maximizing $p(N)$ or, what amounts to the same thing, minimizing:

$$(\delta\xi - \delta\psi)^T K^{-1} (\delta\xi - \delta\psi) \tag{D-12}$$

Differentiating Eq. D-12 with respect to δX_1, and setting the result to 0,

$$\frac{\partial}{\partial(\delta X_1)} \left[(\delta\xi - \delta\psi)^T K^{-1} (\delta\xi - \delta\psi)\right] = - U_{i1}^T K^{-1} (\delta\xi - U\delta X) - (\delta\xi - U\delta X)^T K^{-1} U_{i1} = 0 \tag{D-13}$$

where U_{i1} is the first column of U and thus, an $m \times 1$ column vector. Simplifying Eq. D-13,

$$U_{i1}^T K^{-1} U\delta X + \delta X^T U^T K^{-1} U_{i1} = U_{i1}^T K^{-1} \delta\xi + \delta\xi^T K^{-1} U_{i1} \tag{D-14}$$

Equation D-12 is differentiated with respect to each of the other injection perturbations, and the result is set equal to zero to obtain five more equations similar to Eq. D-14. Combining all six of these equations into one matrix equation,

$$U^T K^{-1} U\delta X + [\delta X^T U^T K^{-1} U]^T = U^T K^{-1} \delta\xi + [\delta\xi^T K^{-1} U]^T \tag{D-15}$$

Since K^{-1} is symmetrical,

$$[U^T K^{-1} U]^T = U^T K^{-1} U \quad \text{and} \quad [K^{-1} U]^T = U^T K^{-1}$$

Equation D-15 becomes

$$U^T K^{-1} U\delta X = U^T K^{-1} \delta\xi$$

or

$$\delta X = J^{-1} U^T K^{-1} \delta\xi \tag{D-16}$$

where

$$J = U^T K^{-1} U \tag{D-17}$$

Equation D-16 gives the solution for the maximum-likelihood estimate of the injection perturbations in terms of the measured coordinates.

The K-matrix in Eq. D-17 is the moment matrix of the noise in all m radio tracking measurements. Thus, K is an $m \times m$ symmetrical matrix, where m is the total number of measurements and may be as large as several thousand. Such a high-order matrix would in general be very difficult to invert. However, as will be shown, the K-matrix in this problem can be approximated by a diagonal matrix.

Let K_{rc} be the element in the rth row and cth column of K. When $r = c$, K_{rc} is the variance of the rth measurement; otherwise, $K_{rc} = K_{cr}$ is the covariance between the rth and cth measurements. If the rth and cth measurements are observations of the same variable at different times, then K_{rc} is the value of the autocorrelation function between the two times; otherwise, K_{rc} is the value of the cross-correlation function between the two times.

It is assumed that there is no correlation between measurements at different stations and between measurements of different types at the same station. Because of the assumption of no cross-correlation, it is possible to partition K into a diagonal matrix of submatrices. Each submatrix K_{pq} is the noise moment matrix for the pth type of data from the qth station. Each U is also partitioned into submatrices U_{pq}, which contain differential coefficients for the pth type of data from the qth station. Thus, Eq. D-17 becomes

$$J = U^T K^{-1} U = \sum_{p,q} U_{pq}^T K_{pq}^{-1} U_{pq} \qquad \text{(D-18)}$$

where J is now the sum of a number of elementary J-matrices, one for each type of data from each station.

With some further assumptions, K_{pq} can be approximated by a diagonal matrix. It is assumed that each type of data from each station is contaminated by n independent noise sources. Each noise source is assumed to have the following idealized autocorrelation function:

$$\begin{aligned} R_n(t) &= \sigma_n^2 \quad \text{for } 0 \leq t \leq \tau_n \\ R_n(t) &= 0 \quad \text{for } t > \tau_n \end{aligned} \qquad \text{(D-19)}$$

That is, the noise is perfectly correlated over an interval τ_n min and is uncorrelated over any larger interval. Assume that the data are sampled at equal time intervals at a rate of f_n samples per minute.

$$S_n = \begin{cases} f_n \tau_n & \text{if } f_n \tau_n \geq 1 \\ 1 & \text{if } f_n \tau_n < 1 \end{cases} \qquad \text{(D-20)}$$

Where S_n is the number of dependent samples in one correlation interval. It can be shown that if the elements of U_{pq} change slowly from one sample time to the next (i.e., there are many samples), then

$$U_{pq}^T K_{pq}^{-1} U_{pq} \simeq C_{pq} U_{pq}^T U_{pq} \qquad \text{(D-21)}$$

where

$$C_{pq} = \left(\sum_n \sigma_n^2 S_n\right)_{pq}^{-1} \qquad \text{(D-22)}$$

The weighting factor C_{pq} takes into account the magnitude and time correlation of the different noise components. For example, if there is only one contaminating noise source, $C = (\sigma^2 S)^{-1}$, and S samples of the data must be taken to have the same weight as one sample of variance σ^2 if the noise were uncorrelated.

It can be seen that by using Eq. D-18, D-21, and D-22, the K-matrix has been approximated by a diagonal matrix. The elements on the diagonal are C_{pq}^{-1}. In the JPL orbit-determination program, the J-matrix is actually calculated as follows:

$$J = \sum_{pq} C_{pq} \left[\sum_i U_i^T U_i\right]_{pq} \qquad \text{(D-23)}$$

The U_i matrix is the 1×6 row vector defined in Eq. D-5, where f_i is now the ith observation of the pth type of data from the qth station. The term in brackets in Eq. D-23 is equal to $U_{pq}^T U_{pq}$. Once K^{-1} is approximated by a diagonal matrix, the method of maximum likelihood becomes the same as the method of least squares. The important difference is in the weighting functions, which account for the correlation in the noise. Thus, using least-square fitting, the expression to be minimized is

$$E^2 = (\delta\xi - \delta\psi)^T K^{-1} (\delta\xi - \delta\psi) \qquad \text{(D-24)}$$

where K^{-1} is diagonal with elements C_{pq}.

To attain the required accuracy in determining δX, the following iterative procedure is used. The injection conditions on the standard preflight trajectory are used for the first iteration. For the second iteration, the preflight standard injection conditions are corrected according to the δX_j's obtained by solving Eq. D-17 in the first iteration. The procedure is repeated until the δX_j's are negligible. It is assumed that the preflight standard is close enough to the actual trajectory so that the method will converge. Normally, sufficient accuracy is attained with 3 or 4 iterations.

It will now be shown that the 6×6 symmetrical matrix J^{-1} specifies the uncertainty in orbit determination due to tracking errors. Substituting Eq. D-8 into D-16,

$$\delta X = J^{-1} U^T K^{-1} \delta\psi + J^{-1} U^T K^{-1} N \qquad \text{(D-25)}$$

The second term in Eq. D-25 is the uncertainty in δX due to noise on the measurements. Let this term be δX_n:

$$\delta X_n = J^{-1} U^T K^{-1} N$$

Then,

$$\delta X_n \, \delta X_n^T = J^{-1} U^T K^{-1} N N^T K^{-1T} U J^{-1T} \qquad \text{(D-27)}$$

Taking the ensemble average of Eq. D-27, noting that $\overline{NN^T} = K$, and using Eq. D-17,

$$\overline{\delta X_n \, \delta X_n^T} = J^{-1} \qquad \text{(D-28)}$$

That is, J^{-1} is the noise moment matrix of the uncertainties in determining the injection conditions. It depends on the differential corrections and on the statistical characteristics of the noise contaminating the radio tracking data.

REFERENCES

1. Jet Propulsion Laboratory, California Institute of Technology. A Method of Describing Miss Distances for Lunar and Interplanetary Trajectories, by W. Kizner. Pasadena, Calif., JPL, 1 August 1959. (EP 674)

2. Jet Propulsion Laboratory, California Institute of Technology. Tracking and Orbit-Determination Program of the Jet Propulsion Laboratory, by R. E. Carr and H. R. Hudson. Pasadena, Calif., JPL, 22 February 1960. (TR 32-7)

3. Tsein, H. S. Engineering Cybernetics. New York, McGraw-Hill, 1954. Pp. 183-88.

4. Jet Propulsion Laboratory, California Institute of Technology. The Statistical Analyses of Space Guidance Systems, by A. R. M. Noton. Pasadena, Calif., JPL, 15 June 1960. (TM 33-15)

5. Jet Propulsion Laboratory, California Institute of Technology. A Description of Deep Space Net Facilities, Operations, and Capabilities, by J. R. Hall. Pasadena, Calif., JPL, 4 December 1959. (P 30-21)

6. Brockman, M. H., et al. "Extraterrestrial Radio Tracking and Communications," Proceedings of the IRE, Vol. 48, No. 4 (April 1960), pp. 643-54.

7. Jet Propulsion Laboratory, California Institute of Technology. Evaluation of Pioneer IV Orbit-Determination Program, by H. Eimer and Y. Hiroshige. Pasadena, Calif., JPL, 22 February 1960. (TR 34-26)

8. Mickelwait, A. B. "Lunar Trajectories," ARS Journal, Vol. 29, No. 12 (December 1959), pp. 905-14.

9. Price, R., et al. "Radar Echoes From Venus," Science, Vol. 129 (1959), p. 751.

10. Jahnke, E., and F. Emde. Tables of Functions. New York, Dover Publications, Inc., 1945. P. 226.

11. Shapiro, I. I. The Prediction of Ballistic Missile Trajectories From Radar Observations. New York, McGraw-Hill, 27 February 1957.